Lithos 296–299 (2018) 297–315

Contents lists available at ScienceDirect

Lithos

journal homepage: www.elsevier.com/locate/lithos

Constraining lithospheric removal and asthenospheric input to melts in Central Asia: A geochemical study of Triassic to Cretaceous magmatic rocks in the Gobi Altai (Mongolia)

Thomas C. Sheldrick [a,*], Tiffany L. Barry [a], Douwe J.J. Van Hinsbergen [b], Pamela D. Kempton [c]

[a] Department of Geology, University of Leicester, University Road, Leicester LE1 7RH, UK
[b] Department of Earth Sciences, Utrecht University, Heidelberglaan 2, 3584 CS Utrecht, The Netherlands
[c] Department of Geology, Kansas State Univeristy, 108 Thompson Hall Manhattan, KS 66506-3201, United States of America

ARTICLE INFO

Article history:
Received 28 August 2017
Accepted 10 November 2017
Available online 21 November 2017

ABSTRACT

Throughout northeast China, eastern and southern Mongolia, and eastern Russia there is widespread Mesozoic intracontinental magmatism. Extensive studies on the Chinese magmatic rocks have suggested lithospheric mantle removal was a driver of the magmatism. The timing, distribution and potential diachroneity of such lithospheric mantle removal remains poorly constrained. Here, we examine successions of Mesozoic lavas and shallow intrusive volcanic plugs from the Gobi Altai in southern Mongolia that appear to be unrelated to regional, relatively small-scale deformation; at the time of magmatism, the area was ~200 km from any active margin, or, after its Late Jurassic-Early Cretaceous closure, from the suture of the Mongol-Okhotsk Ocean. $^{40}Ar/^{39}Ar$ radiometric age data place magmatic events in the Gobi Altai between ~220 to 99.2 Ma. This succession overlaps Chinese successions and therefore provides an opportunity to constrain whether Mesozoic lithosphere removal may provide an explanation for the magmatism here too, and if so, when.

We show that Triassic to Lower Cretaceous lavas in the Gobi Altai (from Dulaan Bogd, Noyon Uul, Bulgantiin Uul, Jaran Bogd and Tsagaan Tsav) are all light rare-earth element (LREE) and large-ion lithophile element (LILE)-enriched, with negative Nb and Ta anomalies ($\frac{Nb}{La}$ and $\frac{Ta}{La} \leq 1$). Geochemical data suggest that these lavas formed by low degrees of partial melting of a metasomatised lithospheric mantle that may have been modified by melts derived from recycled rutile-bearing eclogite. A gradual reduction in the involvement of garnet in the source of these lavas points towards a shallowing of the depth of melting after ~125 Ma.

By contrast, geochemical and isotope data from the youngest magmatic rocks in the area — 107-99 Ma old volcanic plugs from Tsost Magmatic Field — have OIB-like trace element patterns and are interpreted to have formed by low degrees of partial melting of a garnet-bearing lherzolite mantle source. These rocks did not undergo significant crustal contamination, and were derived from asthenospheric mantle. The evidence of a gradual shallowing of melting in the Gobi lava provinces, culminating in an asthenospheric source signature in the youngest magmatic rocks is similar to examples from neighboring China, emphasising the wide-scale effect of a regional Mesozoic magmatic event during similar time periods. We suggest that Mongolia underwent lithospheric thinning/delamination during the Mesozoic (between ~125 and ~107 Ma) with patchy areas thinning sufficiently to enable the generation of relatively small-scale asthenospheric-derived magmatism to predominate in the late Cretaceous.

1. Introduction

Mesozoic mafic-intermediate magmatic rocks crop out over an estimated 9800 km^2 across southern and eastern Mongolia (Fig. 1A). The Mesozoic magmatism stretches from the Greater Xing'an Mountains in northeast China to far-east Russia (e.g., Badarch et al., 2002; Dash et al., 2015; Fan et al., 2003; Meng, 2003; Van Hinsbergen et al., 2008, 2015; Wang et al., 2006; Yarmolyuk and Kovalenko, 2001), largely within a Neoproterozoic to Mesozoic orogen known as the Central Asian Orogenic Belt (CAOB) (e.g., Windley et al., 2007; Xiao et al., 2015 and references therein). This widespread, low-volume magmatism is located within the east Asian continental interior, far away from continental margins, and its cause remains enigmatic.

Magmatism is often linked to plate boundary processes, either subduction or rifting and spreading, but such an explanation for the

* Corresponding author.
E-mail address: ThomasSheldrick@gmail.com (T.C. Sheldrick).

https://doi.org/10.1016/j.lithos.2017.11.016

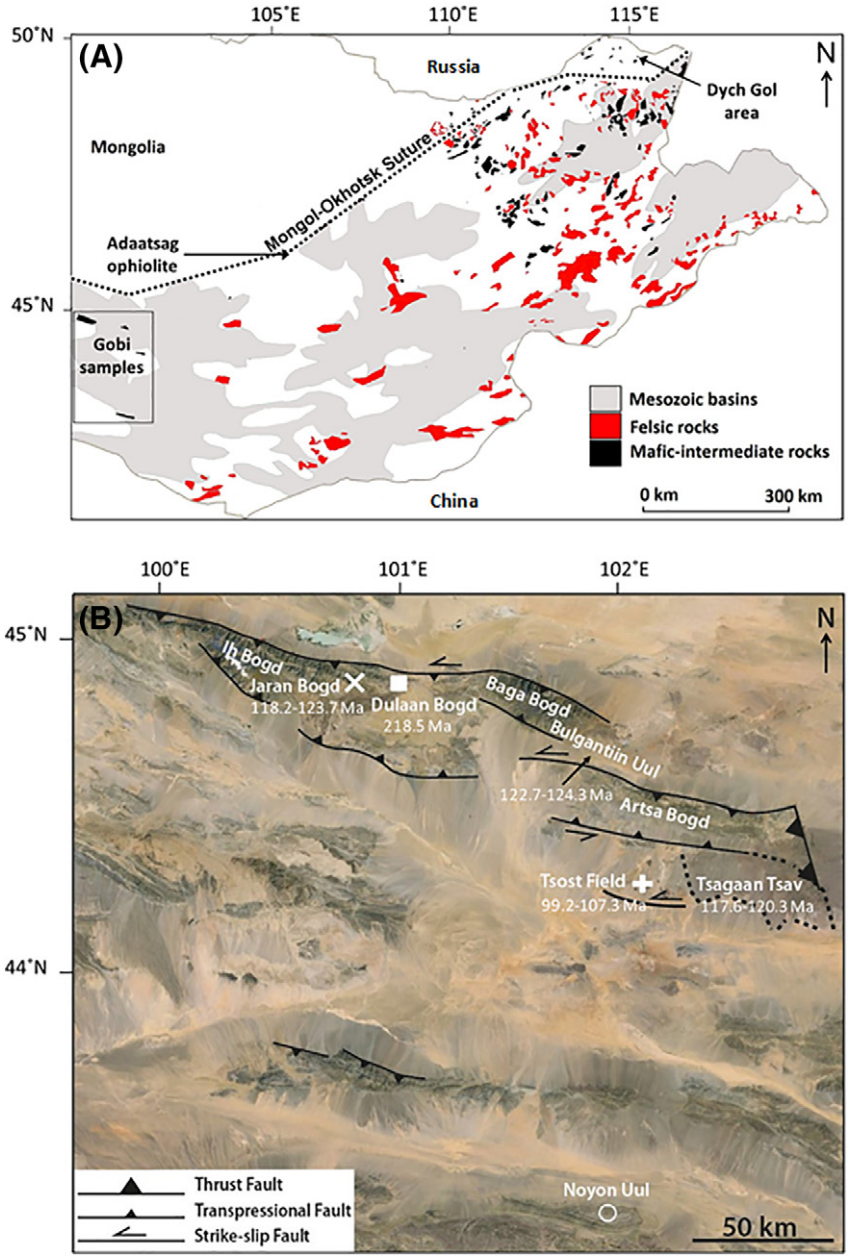

Fig. 1. (A) A sketch map of Mongolia showing the sample area (boxed area) and the distribution of Mesozoic mafic to intermediate lavas. Felsic magmatism is also shown, but age relationships are often not established. The distribution of volcanism is based on Mongolian government geological maps and field observations. The distribution of Mesozoic sedimentary basins is from Johnson et al. (2003). (B) A portion of the Gobi Altai showing our field localities (Google Earth). Information on the distribution of faults is taken from Van Hinsbergen et al. (2008).

magmatism of central Asia is problematic. Most of the formation of the CAOB occurred via subduction processes in the Palaeozoic, which came to a halt in the Triassic (e.g., Xiao et al., 2015). Subduction of Paleo-Pacific lithosphere in the east, or Neotethys lithosphere in the south, occurred >2000 km away from Mongolian Mesozoic lava fields (e.g., Torsvik and Cocks, 2017; Van Hinsbergen et al., 2015). The Mongolian Mesozoic magmatism often appears to be spatially and temporally related to the widespread formation of extensional sedimentary basins (e.g., Meng, 2003; Johnson et al., 2014; Van Hinsbergen et al., 2015). Interbedded sedimentary and basaltic successions in some of the Mongolian Mesozoic extensional basins reach up to 3 km in thickness (Graham et al., 2012), but these large cumulative thicknesses of Mesozoic magmatism are inconsistent with the existence of only relatively small-scale (half)-grabens that would have accommodated no more than a few kilometres of extension (e.g., Johnson et al., 2014; Van Hinsbergen et al., 2015). Therefore, while this regional extension may be related to the same geodynamic process that caused the volcanism, the small magnitude of the extension makes it unlikely to have been the cause of the magmatism. The only plate boundary that was active in the vicinity of the Mongolian magmatic fields during the earlier part of their formation was the subduction zone associated with the closure of the Mongol-Okhotsk Ocean, which was active until latest Jurassic - earliest Cretaceous time (Cogné et al., 2005; Van der Voo et al., 2015). Yet this boundary was distant from the penecontemporaneous magmatism in the North China Craton where volcanic rocks and xenolith data have led to suggestions for widespread lithosphere removal during the Mesozoic (e.g., Gao et al., 2002; Menzies et al., 1993; Windley et al., 2010). Within Mongolia, the presence of Mesozoic extensional basins, A-type granites and extensive mafic, and subordinate felsic volcanism have been suggested as evidence for similar

lithospheric delamination processes (e.g., Dash et al., 2015; Graham et al., 2001; Jahn et al., 2009; Windley et al., 2010). Other explanations for (or part of) the regional magmatism include mantle plume activity (Yarmolyuk and Kovalenko, 2001), slab breakoff in the Mongol-Okhotsk region (Meng, 2003), or a combination of delamination, very distant back-arc extension, and mantle upwelling induced by mantle avalanching of previously subducted slabs around the Asian continents (Dash et al., 2015).

In this study, we investigate the petrogenesis of Mesozoic magmatic rocks in southern Mongolia to constrain the nature of the source of the magmatism, the timing of magmatic activity, and the implications of the timing and changes in source chemistry for understanding underlying lithospheric controls. We focus on an area in the Gobi Altai, located south of the western end of the Mongol-Okhotsk Suture (Fig. 1B), where well-dated, well-described basaltic successions span the long duration of Triassic to the Late Cretaceous, straddling the latest Jurassic-earliest Cretaceous closure, ~200 km to the north of the study area, of the Mongol-Okhotsk Ocean that once extended between the Siberian and the Mongol-China terranes/crustal blocks (Cogné et al., 2005; Van der Voo et al., 2015).

2. Geological setting and sampling

The terranes that comprise northeast China and Mongolia have been amalgamated and, to varying degrees, affected by subduction processes during the closure of the Paleo-Asian Ocean throughout the Palaeozoic to Early Triassic (Şengör et al., 1993; Xiao et al., 2015). Geochemical traces of these processes are likely still reflected in the composition of the Asian continental crust and mantle lithosphere. The latest stages of amalgamation concerned the Triassic formation of the Solonker suture, ~500 km to the south of the Gobi Altai (Xiao et al., 2015), and the Mongol-Okhotsk suture, 150–200 km to the north (Van der Voo et al., 2015). After the Jurassic, the nearest plate boundaries were the Paleo-Pacific and Neo-Tethys subduction/collision zones, >2000 km away (e.g., Yin and Nie, 1996; Taira, 2001; Cunningham, 2013; Van Hinsbergen et al., 2015).

The Mongol-Okhotsk Ocean formed in the Carboniferous (e.g., Cocks and Torsvik, 2007; Kravchinsky et al., 2002; Tomurtogoo et al., 2005) between the continental blocks of Siberia to the north and Amuria (Mongolia) - North China blocks to the south, and closed in the latest Jurassic-earliest Cretaceous time (e.g., Van der Voo et al., 2015). The remnants of this paleo-ocean are evident within the Mongol-Okhotsk suture where a band of ophiolites (Tomurtogoo et al., 2005) and marine fossil-bearing sediments (Halim et al., 1998) track NE-SW across central Mongolia. Unexpectedly, perhaps, for such a large-scale continental collision, the suture is not characterized by any topographic highs. It is also unclear where the suture terminates, or whether it can be identified west of ~100°E (e.g., Fritzell et al., 2016; Van der Voo et al., 2015). Subduction-related magmatism appears to occur on both sides of the Mongol-Okhotsk suture (Zorin, 1999). This observation led to the suggestion that subduction occurred both northwards and southwards, beneath Siberia and Amuria, respectively (e.g., Windley et al., 2010) which is also consistent with seismic topography by Van der Voo et al. (2015).

Regardless of the direction of subduction, palaeomagnetic data (e.g., Cogné et al., 2005; Kravchinsky et al., 2002; Van der Voo et al., 2015) suggest the final closure of the Mongol-Okhotsk Ocean occurred between the Late Jurassic (~155 Ma) and the beginning of the Early Cretaceous (~120 Ma). This event was followed by periods of extension that formed large basins within southern Mongolia and China (e.g., Graham et al., 2001; Johnson, 2015; Meng, 2003). These extensional basins, such as the East Gobi basin in the Gobi Altai, were intermittently filled with volcanic rocks and sedimentary units. Within, and adjacent to, the East Gobi basin, are isolated exposures of these Mesozoic basaltic magmatic rocks, which are particularly well exposed within the Ih Bogd, Baga Bogd and Artsa-Bogd mountains of the Gobi Altai (Figs. 1B & 3). These isolated mountain ranges are Miocene to recent flower-structures that formed at restraining bends along the large, left-lateral Bogd strike-slip fault system (Cunningham, 2013 and references therein).

The Gobi Altai magmatism has undergone minimal weathering and samples were collected from six locations, from west to east: Jaran Bogd, Dulaan Bogd, Bulgantiin Uul, Noyon Uul, Tsagaan Tsav, and the Tsost Magmatic Field (Fig. 1B). The Tsost Magmatic Field is comprised of a series of intrusive basalts, interpreted as shallow plugs and dykes (Barry, 1999), but otherwise, all the other studied basaltic rocks appear to be extrusive lavas and perhaps intervening sills (Barry, 1999; Van Hinsbergen et al., 2008, 2015). We will refer to the latter as the Gobi lavas throughout this paper.

Ih Bogd, Baga Bogd and Artsa Bogd expose crystalline Palaeozoic basement that has been affected by sedimentation, magmatism, and metamorphism related to subduction, obduction, and collisions during the formation of the CAOB (e.g. Badarch et al., 2002; Xiao et al., 2015). These localities are unconformably overlain by up to 1500 m of Mesozoic mafic volcanic rocks that are interbedded with fluvial sandstones and lacustrine clay deposits (Van Hinsbergen et al., 2015 and references therein). From west to east, the lavas have been dated by ^{40}Ar-^{39}Ar geochronology; the Jaran Bogd sequence gave ages ranging from ~125 to 118 Ma; Dulaan Bogd yielded an age of 218.5 ± 1.5 Ma; and those from the Bulgantiin Uul sequence yielded ages of 124.3 ± 0.9 and 122.7 ± 0.8 Ma (Van Hinsbergen et al., 2008, 2015). Results from ^{40}Ar-^{39}Ar age dating for Tsost Magmatic Field and Tsagaan Tsav were provided in the PhD thesis of Barry (1999), but were never formally published, and are presented below. Previous K-Ar results for Tsost Magmatic Field gave an age of ~101 to 76 Ma, and the lavas from Tsagaan Tsav gave an age between 95 and 90 Ma (Samoylov and Arkelyants, 1989; Enkhtuvshin et al., 1995). No age constraints are available for Noyon Uul in the south.

Other than the volcanic rocks at Noyon Uul, the lavas and shallow plugs are all situated within the Gobi Altai terrane (Badarch et al., 2002), which is a long narrow belt extending east into China. This terrane was interpreted as a former backarc/forearc basin containing greenschist facies rocks of Cambrian age. In the far south of the area, Noyon Uul sits on the Atasbogd terrane, which is described as a backarc/forearc basin terrane containing greenschist facies rocks of Ordovician age. Noyon Uul is a syncline and the dominant strata consist of fluvial and lacustrine facies sedimentary rocks of Upper-Permian-Lower Jurassic age (Hendrix et al., 1996).

3. Petrography

The Gobi lavas are porphyritic, vesicular and contain amygdales of carbonate and siliceous material. All Dulaan Bogd samples are holocrystalline while Bulgantiin Uul, Jaran Bogd and Tsagaan Tsav samples are holo- to hypocrystalline. All the Noyon Uul samples are hypocrystalline. There are phenocrysts of plagioclase, clinopyroxene and iddingsitised olivine. Glomerocrysts of altered olivine and clinopyroxene were identified in samples from Bulgantiin Uul, Jaran Bogd and Tsagaan Tsav. Rare xenocrysts of plagioclase crystals were identified in Bulgantiin Uul samples. The groundmass consists of iddingsitised olivine, clinopyroxene, plagioclase, opaque crystals and in some cases glass. There are samples from all magmatic provinces that have flow-aligned plagioclase crystals. Clinopyroxene subophitically encloses plagioclase in Jaran Bogd, Bulgantiin Uul and Tsagaan Tsav lavas. The Noyon Uul lavas also contain accessory apatite. In all samples olivine is fully or partially altered to iddingsite, whereas clinopyroxene and plagioclase are partially altered. Overall, Dulaan Bogd, Bulgantiin Uul and Jaran Bogd lavas are the least altered (approximately 2 to 32% altered), whereas Noyon Uul and Tsagaan Tsav lavas are the most altered (approximately 10 to 40% altered). Most of this alteration is of specific phases; however, localized groundmass and glass alteration occurs in samples from all magmatic provinces.

Tsost Magmatic Field basalt samples are porphyritic, holocrystalline and hypocrystalline, contain amygdales of zeolites and are generally

fresher than the other sample localities (approximately 1 to 18% altered). There are phenocrysts of plagioclase, clinopyroxene and iddingsitised olivine (many only partially altered). Clinopyroxene and olivine crystals appear as glomeroporphyritic clusters. Skeletal hopper olivine crystals suggest quenching happened despite these basalts being intrusive. The groundmass consists of olivine, clinopyroxene, plagioclase feldspar, opaque crystals and, in some cases, glass.

Granulite crustal xenoliths were observed at Tsagaan Tsav and more rarely in Tsost Magmatic Field, but the latter also contains xenoliths consisting of plagioclase and pyroxene crystals.

Photomicrographs and detailed sample specific petrological descriptions for each volcanic field are reported in the supplementary appendix material (Supplementary Material A).

4. Argon dating

Three samples were selected from Tsost Magmatic Field for whole-rock $^{40}Ar/^{39}Ar$ dating; two samples were from plug-like intrusions (TB95-6.3.3 and TB95-7.1.6) and the third, TB95–9.5.2, was from an E-W trending dyke which lay between two of the volcanic plugs. Three lavas were also selected from Tsagaan Tsav for whole-rock $^{40}Ar/^{39}Ar$ dating (TB95-8.2, TB95-8.7 and TB95-11.6). The samples were selected based on high total alkalis ($K_2O + Na_2O$), freshness of feldspar phenocrysts, and minimal glass content. The analytical procedure and Ar-Ar recalculations are reported in the Supplementary Material B & C.

The determined ^{40}Ar-^{39}Ar ages constrain the lavas from Tsagaan Tsav between 120.4 ± 1.1 and 117.7 ± 1.7 Ma. The shallow intrusive plugs from Tsost Magmatic Field yield the youngest ages from the Gobi Altai region, with ages between 107.4 ± 0.9 and 99.3 ± 0.8 Ma (Fig. 2).

5. Geochemistry of the Gobi lavas and intrusives

5.1. Major-element variations

Petrological observations reported above indicate that most phenocrysts and groundmass material had undergone at least some alteration.

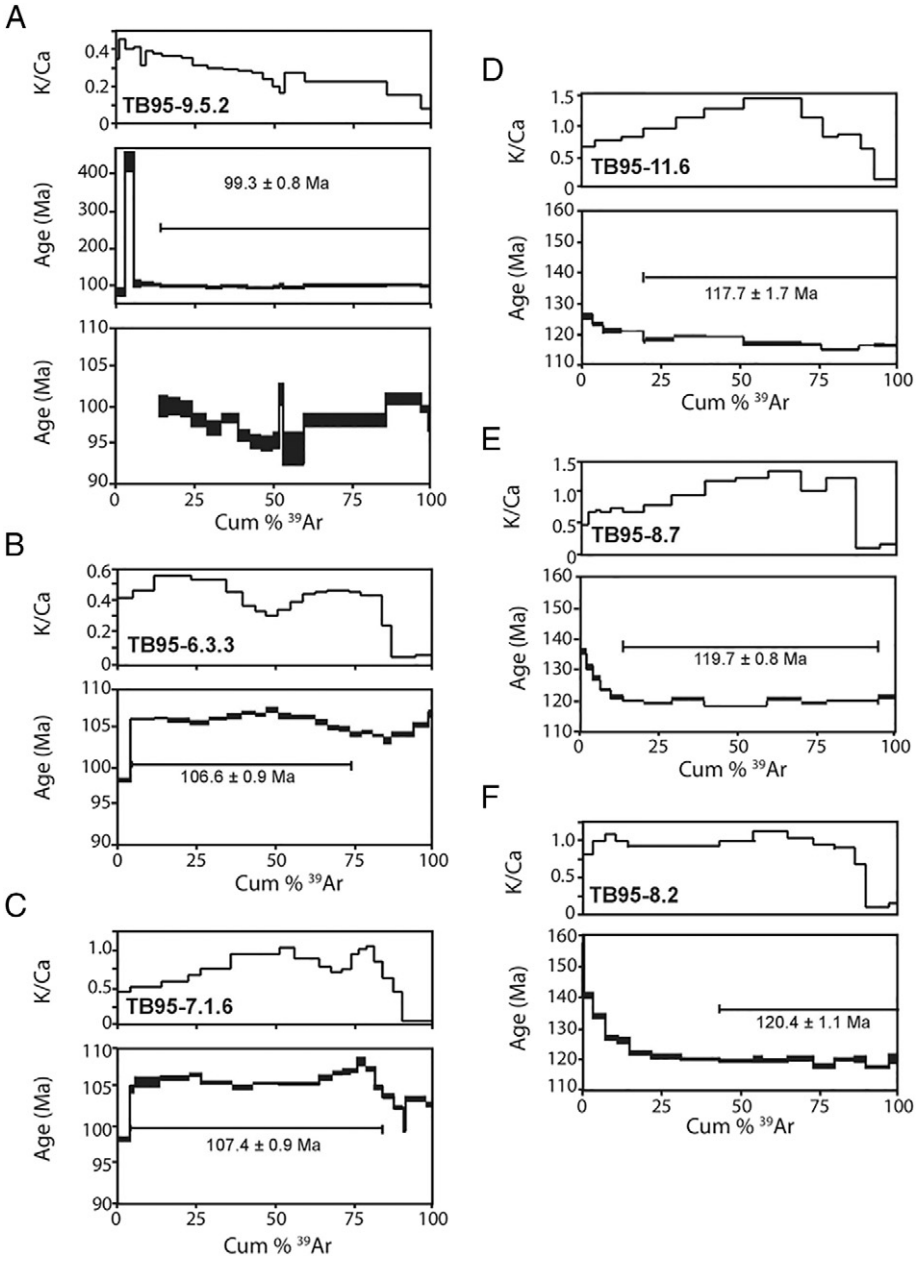

Fig. 2. Whole-rock recalculated $^{40}Ar/^{39}Ar$ age plateau diagrams for Tsost Magmatic Field (A-C) and Tsagaan Tsav (D-F).

More than half the samples studied have <2 wt% LOI (loss on ignition) values, suggesting they have not undergone extensive alteration. All of the Noyon Uul samples have LOI values >2 wt%, whereas the other lava fields show evidence for more variable degrees of alteration. LOI versus trace-element plots show that many mobile elements (e.g. Rb, Ba, Pb, Na) have been affected by alteration and these are included in the supplementary appendix material (Supplementary Material D).

To classify the alkaline lavas and intrusive rocks a Total Alkali Silica (TAS) plot is used (Fig. 3). Tsost Magmatic Field samples plot in the trachybasalt and basaltic trachyandesite fields. Most of the localities exhibit a similar range in composition, with the majority of samples plotting in the basaltic trachyandesite field. Some samples from Noyon Uul, Bulgantiin Uul and Tsagaan Tsav plot in the basanite (8 samples) or phonotephrite (2 samples) fields. On a normative Ne-Ol-Di-Hy-Qz diagram, most of the samples plot in the nepheline-normative and hypersthene-normative fields, but 12 samples plot in the quartz-normative field (Fig. 4A). However, the samples that plot in the quartz-normative field have low amounts of MgO (<3 wt%) and a clear trend can be seen for some volcanic provinces (Tsost Magmatic Field, Jaran Bogd and Dulaan Bogd) going from nepheline-normative to quartz-normative as the melts become increasingly evolved (Fig. 4B).

Samples are variably evolved with MgO contents ranging from 0.44 to 8.25 wt% depending on locality: Tsost Magmatic Field basalts have Mg-numbers between 43 and 68. Excluding Noyon Uul, the lavas have Mg-numbers between 27 and 56 (Fig. 5); Noyon Uul samples have Mg-numbers between 7 and 33. Generally $Fe_2O_{3\ (T)}$ does not vary as a function of Mg-number, except for Noyon Uul samples, which show a negative trend with increasing Mg-number (Fig. 5C). Samples from all locations show a positive trend between Mg-number and CaO contents, and CaO/Al_2O_3 ratios (Fig. 5F & I).

5.2. Trace-element and REE variations

Cr contents correlate positively with Mg-number (Fig. 5H). Tsost Magmatic Field basalts have the highest Cr concentrations with values ranging from 89 to 219 ppm, while Dulaan Bogd lavas have 47 to 177 ppm, Noyon Uul 6 to 110 ppm, Bulgantiin Uul 10 to 51 ppm, Jaran Bogd 17 to 187 ppm and Tsagaan Tsav 27 to 34 ppm.

Ni concentrations also increase with Mg-number (Fig. 5G). Tsost Magmatic Field basalts have Ni concentrations between 59 and 98 ppm, while Dulaan Bogd lavas have values between 16 and 127 ppm, Noyon Uul 17 to 51 ppm, Bulgantiin Uul 10 to 50 ppm, Jaran Bogd 22 to 147 ppm and Tsagaan Tsav 34 to 45 ppm.

All samples are enriched in the light rare earth elements (LREE) compared to normal mid-ocean ridge basalt (N-MORB) compositions and have elevated LREE relative to heavy rare earth elements (HREE).

Primitive mantle-normalized diagrams (Fig. 6) show that the samples are enriched in the high field strength elements (HFSE) and the large ion lithophile elements (LILE) compared with N-MORB. However, the LILE are susceptible to alteration and given the degree of alteration of most samples (described above), original concentrations may have been changed. With the exception of Tsost Magmatic Field basalts, the lavas show prominent negative Nb and Ta anomalies, a feature commonly observed in island-arc volcanics, along with enrichment in the fluid-mobile incompatible trace elements such as the LILE (e.g., Rb, Ba, K). Throughout the sample suites, some samples have positive Ba, Pb and Zr anomalies, but these are less prominent in the Tsost Magmatic Field basalts. Some lavas also have negative Sr and Ti anomalies. However, unlike volcanic arc lavas, the Gobi samples are enriched in incompatible trace elements like Zr. Similarities between an average continental arc basalt (CAB; Fig. 6 B–F) and the Southern Basin-and-Range (USA; Fig. 6G) lavas with the Gobi lavas are seen in the mirroring of positive and negative anomalies. This enrichment of Rb, Ba and K in the Basin-and-Range lavas has been attributed to melting of metasomatised lithospheric mantle (e.g., Fitton et al., 1991; Kempton et al., 1991). The lack of a negative Nb and Ta anomaly and a much weaker positive Pb anomaly for Tsost Magmatic Field basalts is comparable to ocean island basalt (OIB; Fig. 6A).

6. Data interpretation

6.1. Fractional crystallization

The correlation of Cr and Ni with Mg-number likely reflects fractionation of olivine and Cr-spinel; in addition, fractionation of clinopyroxene is evident from decreasing CaO/Al_2O_3 ratios with Mg-number (Fig. 5I). Such a fractionation assemblage is supported by petrological observations which show olivine and clinopyroxene as the most common phenocryst phases. There does not seem to have been significant plagioclase fractionation for Tsost Magmatic Field basalts as shown by chondrite normalized Eu/Eu* numbers ($Eu/Eu^* = \frac{Eu_N}{Sm_N + Gd_N\ 0.5}$) ranging from 0.98–1.06. However, most of the other volcanic provinces exhibit negative Sr anomalies on

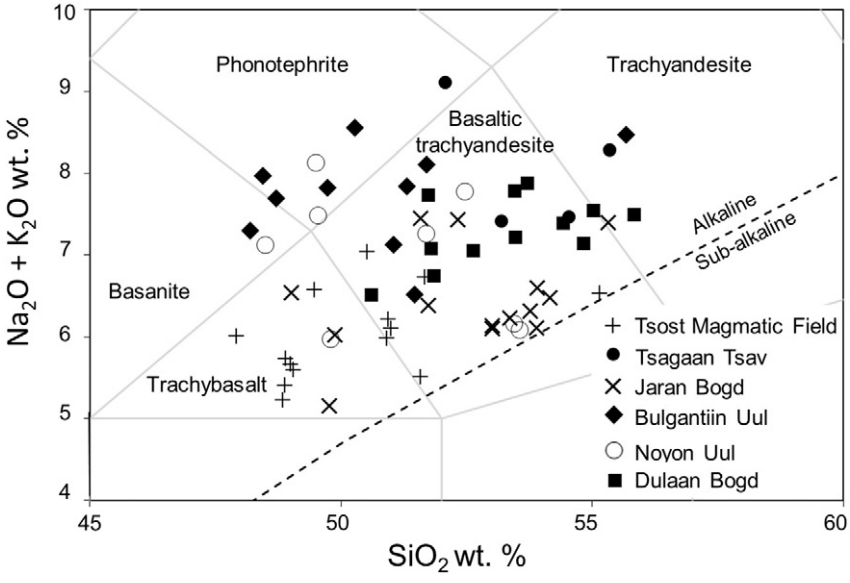

Fig. 3. A Total Alkali Silica (TAS) diagram from LeBas et al. (1986) with the alkaline and sub-alkaline dividing line from Irvine and Baragar (1971) also shown.

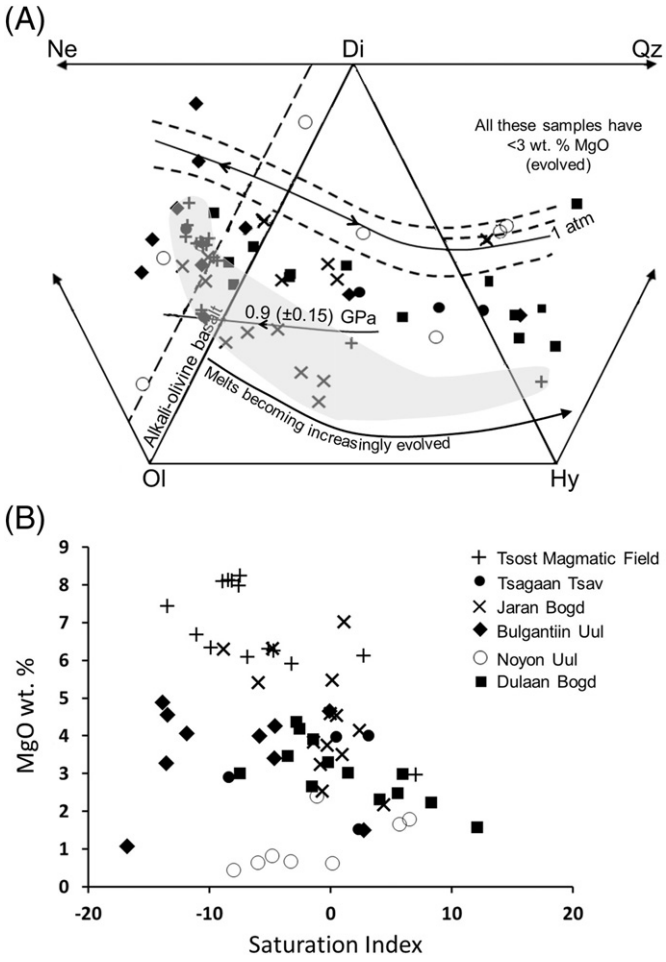

Fig. 4. (A) a normative Ne-Ol-Di-Hy-Qz diagram using $Fe_2O_3/FeO = 0.2$. 1 atm and 0.9 GPa cotectics from Thompson et al. (2001); arrows point in the direction of decreasing temperature. The majority of samples plot below the 1 atm bar. The shaded area shows where the Tsost Magmatic Field basalts plot and also highlights that many of the Jaran Bogd lavas show a similar distribution. (B) Saturation index (SI) versus MgO plot. SI = $100(Si-(Al + Fe^{2+} + Mg + 3Ca + 11Na + 11K + Mn - Fe^{3+} - Ti - 4P)/2)$ where Si, Al etc. are weight percent oxides divided by their respective molecular weights (Fitton et al., 1991). Fe_2O_3 wt% was calculated from total Fe using $Fe_2O_3/(Fe_2O_3 + FeO) = 0.2$. Critically saturated basalts (neither hy- nor ne-normative) have SI = 0; under-saturated compositions (ne-normative) have SI < 0; saturated to over-saturated basalts have SI > 0.

primitive mantle plots and have Eu/Eu* numbers ranging from 0.72–0.83 for Dulaan Bogd, 0.76–0.81 for Noyon Uul, 0.78–0.87 for Bulgantiin Uul, 0.74–0.97 for Jaran Bogd and 0.80–0.87 for Tsagaan Tsav, indicative of varying degrees of plagioclase fractionation. The presence of opaque minerals identified during petrological studies suggests fractionation of oxides. As the lavas and basalts from Dulaan Bogd, Jaran Bogd and Tsost Magmatic Field become increasingly evolved they move from the nepheline-normative to the quartz-normative fields (Fig. 4A & B). Because the Gobi samples are evolved (most samples <5 wt% MgO), it is difficult to assess whether the trend from nepheline-normative to quartz-normative is because of fractionation processes at moderate pressures (5–10 kb), crustal contamination, or simply because the normative mineralogy calculation for the evolved samples is not suitable (Chakraborty, 1980). However, it is interesting that many Jaran Bogd samples follow a similar trend to Tsost Magmatic Field samples, perhaps indicating similar fractionating conditions or some sort of mixing process.

Amphibole was not observed as a phenocryst or groundmass phase, and a Dy/Yb vs. SiO_2 wt% plot (Fig. 7A) shows that each volcanic province has trends consistent with clinopyroxene fractionation, rather than amphibole involvement. For comparison, Cenozoic basalts from Mongolia (Togo) which have had a combination of garnet (high Dy/Yb ratios) and amphibole involvement in the source are also plotted (Barry et al., 2003; Hunt, 2011). Unlike the Gobi samples, the Togo basalts have decreasing Dy/Yb ratios with increasing SiO_2 wt%, consistent with amphibole involvement.

The negative Nb, Ta and Ti anomalies on the primitive mantle-normalized plots (Fig. 6) suggest these lavas could have fractionated or interacted with residual rutile; alternatively, these geochemical attributes could be a source feature. If rutile was involved, then given that the minimum pressure stability of rutile is about 1.5 GPa, this would equate to a minimum depth of origin for the lavas of about 45–50 km (Xiong et al., 2005). Rutile fractionates Nb (Kd = ~28) from Ta (Kd = ~36), resulting in high Nb/Ta ratios in a melt derived from a rutile-bearing source; rutile dissolves when temperatures exceed 1250 °C at 2–3 GPa (e.g., Bennett et al., 2004; Foley et al., 2000; Klemme et al., 2005; Xiong et al., 2005). If the source has high Nb/Ta ratios due to a fractionating phase like rutile, or because it has been modified by metasomatism, then any melt from such a source could also have high Nb/Ta ratios. Melts of rutile-free peridotite mantle, without recycled continental crust involvement, will be characterized by Nb/Ta ratios close to values for primitive mantle (17.39; Sun and McDonough, 1989). The Nb/Ta ratios for Tsost Magmatic Field basalts range from 15.8 to 20.6 (average of 17.3 ± 1.4), similar to primitive mantle, whereas the Gobi lavas have more variable ratios (12.8 to 38.9; average of 22.6 ± 6.5). Average continental crust has Nb/Ta ratios of 10.9 (Rudnick and Fountain, 1995) and therefore the ratios in the Gobi samples are unlikely to be explained by crustal contamination. Both Nb and Ta are also compatible in ilmenite and spinel, with Ta being more compatible then Nb; thus, fractionation of these oxides would also result in higher Nb/Ta ratios in the residual liquid.

To consider whether fractionation of these oxides can explain the ratios seen in the Gobi samples, a simple Rayleigh fractional crystallization ($\frac{C_l}{C_0} = F^{D-1}$) model is considered (Fig. 7B). To test whether the Gobi lavas are evolved versions of a melt similar to Tsost Magmatic Field basalts, but with Nb and Ta anomalies developed by fractionation of Fe-Ti oxides (ilmenite and spinel), the starting composition will use Nb = 38 ppm and Ta = 2.3 ppm based on sample TB95-6.3 (from Tsost Magmatic Field), as this sample has the most MgO and therefore is one of the least evolved. The partition coefficients (Kd) vary from 0.55 to 1.9 for Nb and 0.95 to 2.7 for Ta (Klemme et al., 2006). Two fractionation trends are considered, using the lowest and highest Kd values for Nb and Ta. To model the average Nb/Ta ratio of 22.6 using the smallest Kd values, ~58% fractionation of Fe-Ti oxides would be required, resulting in a positive correlation between Nb and Nb/Ta ratios. Alternatively, assuming the highest Kd values, ~36% fractionation would be required, resulting in a negative correlation between Nb and Nb/Ta. Therefore, both models require unreasonably large amounts of fractionation. Thus, fractionation of ilmenite/spinel may have helped elevate Nb/Ta ratios but can't be solely responsible for the high ratios in the lavas.

Considering that the high Nb/Ta ratios are unlikely to be explained by crustal contamination or fractionation of ilmenite/spinel, this leaves rutile fractionation or source controls as possible explanations.

It has been suggested by Klemme et al. (2002) that TiO_2 in an eclogite protolith will need to be > 1.6 wt% for rutile saturation in the melt derived from the eclogite (at 3 GPa). Therefore the protolith will need to contain sufficient TiO_2 to stabilize rutile. Any interaction between a Ti-rich melt and mantle peridotite may lower the TiO_2 enough to prevent rutile fractionation, and it is argued in later sections that peridotite is the dominant source lithology. Mesozoic lavas (>110 Ma) from the North China Craton show similar negative Nb and Ta anomalies and high Nb/Ta ratios. Rutile fractionation was ruled out for these high MgO (>10 wt%) lavas because there is a negative correlation between MgO and Nb and Ta (Liu et al., 2008). This suggests that both Nb and Ta were incompatible during mantle melting. Instead, the geochemical features were attributed to source controls. Given the similar age of the Gobi lavas, they may have similar petrologic histories. Furthermore, none of the Gobi lava fields have

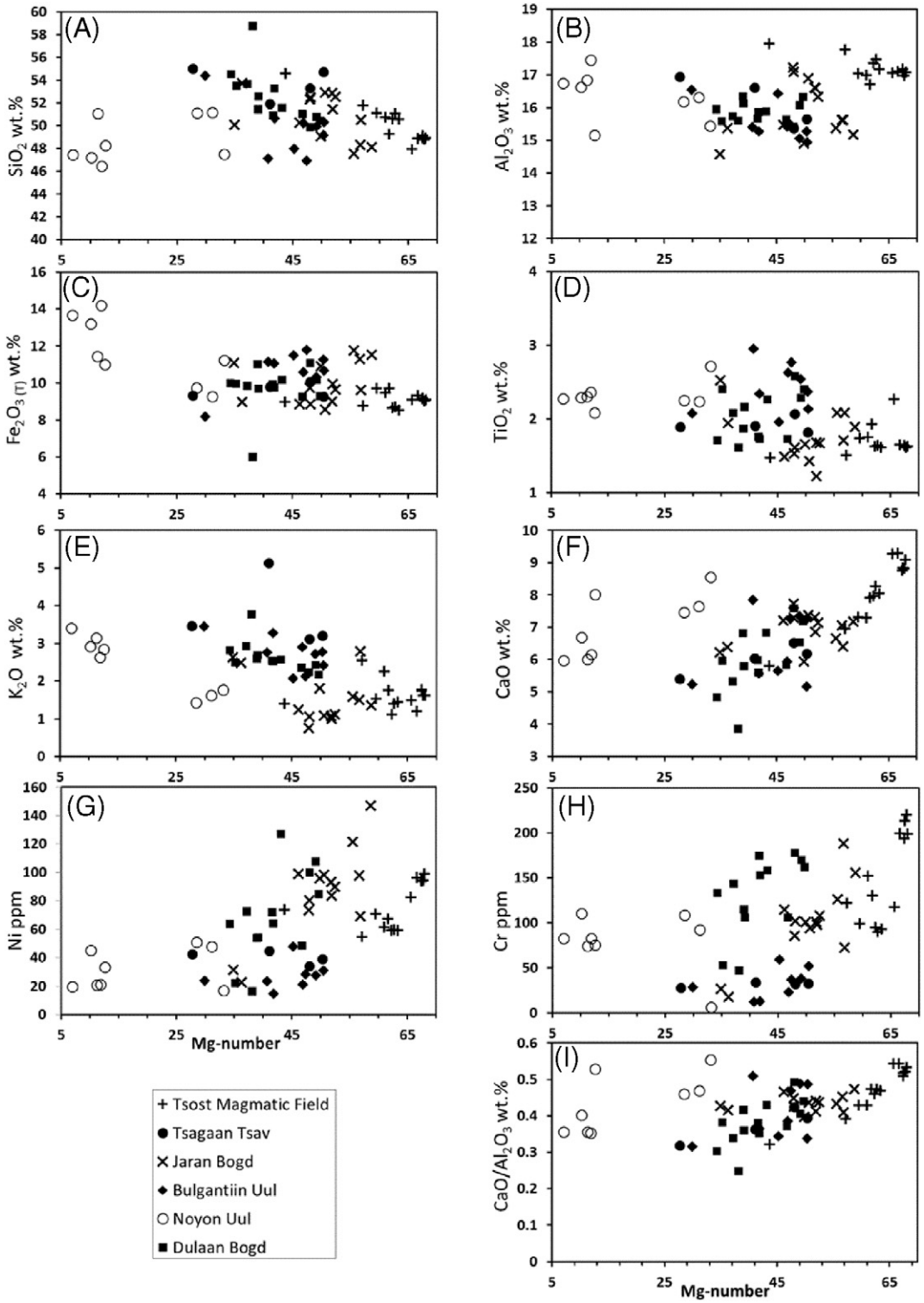

Fig. 5. Variations in major-element oxides, compatible trace elements and CaO/Al_2O_3 with Mg-number (Mg-number $(100 \times (\frac{MgO}{40.3}) \Big/ \left((\frac{MgO}{40.3}) + (\frac{FeO}{71.85})\right)$ is calculated using a Fe_2O_3/FeO ratio of 0.2 ($FeO = \left(\frac{Fe_2O_{3(T)}}{(1+(\frac{0.2}{1.111}))}\right) \Big/ 1.111$).

decreasing Nb with MgO, consistent with the likelihood that there has not been rutile fractionation (Supplementary Material D).

If rutile is unlikely to have been a fractionating phase, then it is likely that the low Nb and Ta concentrations, and high Nb/Ta ratios are controlled by source characteristics. There are a number of ways this source could be generated for the Gobi lavas (or a combination of reasons): (1) interaction between mantle peridotite and a melt derived from a rutile-bearing, recycled eclogite (e.g., Liu et al., 2008); (2) the involvement of previous subducted continental crust trapped in the lithospheric mantle (e.g., Fan et al., 2004) and (3) interaction between mantle peridotite and fluids with high concentrations of LREE but depleted in Nb and Ta. Peridotite xenoliths with melt pockets have been found in Cenozoic alkali basalts from Mongolia (Ionov et al., 1994). It was shown that the invading fluids were enriched in LREE, Th, U, Pb and Sr

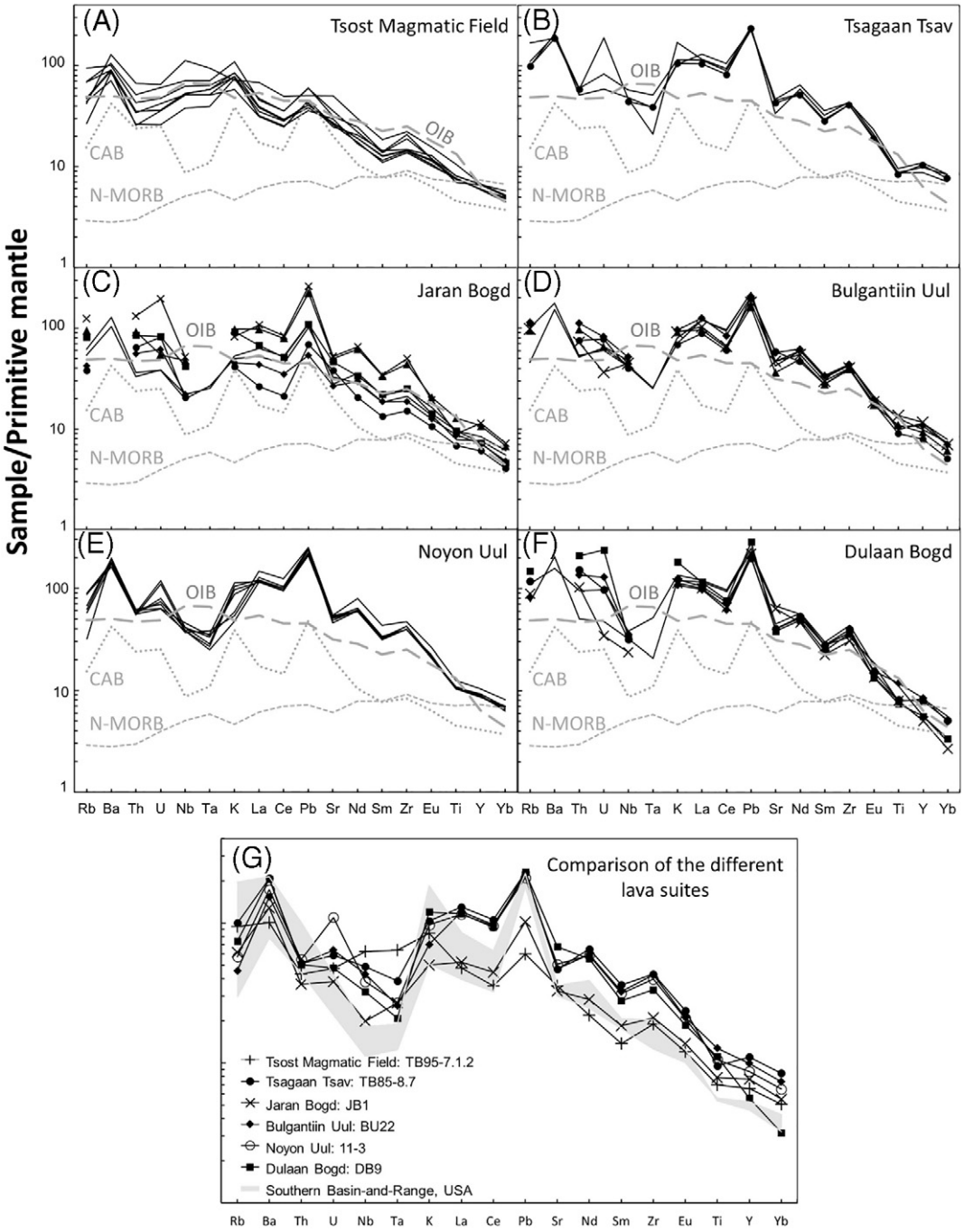

Fig. 6. Primitive mantle-normalized trace element variation diagrams for the different lava suites. Normalization values for the primitive mantle from Sun and McDonough (1989) and the Pb normalization value used was 0.071. Data sources: average N-MORB: Gale et al. (2013); average OIB: Sun and McDonough (1989); average CAB: Kelemen et al. (2003); southern Basin-and-Range basaltic volcanism from Bradshaw et al. (1993).

while also depleted in Nb and Ta, having high Nb/Ta ratios. Thus, considering xenoliths from Mongolia show a mantle enriched by metasomatism events, coupled with the similar age between the Gobi lavas and Chinese lavas (>110 Ma), it seems likely the negative Nb and Ta anomalies (Fig. 6) and high Nb/Ta ratios are a source characteristic, reflecting modified lithospheric mantle.

6.2. Isotope variations and crustal contamination

Tsost Magmatic Field basalts have low $^{87}Sr/^{86}Sr_{(i)}$ isotopic ratios (0.7034–0.7041) and relatively high $^{143}Nd/^{144}Nd_{(i)}$ isotopic ratios (0.5126-0.5127; $\varepsilon_{Nd(t)} = 3.3–4.88$). This is similar to the Dych Gol lavas from Mongolia ($^{87}Sr/^{86}Sr_{(i)} = 0.704–0.7043$ and $^{143}Nd/^{144}Nd_{(i)} = 0.5126–0.5127$) which are also of a similar age to Tsost Magmatic Field basalts ($^{40}Ar/^{39}Ar$; 104.7 Ma ± 0.3 Ma) and were interpreted to be derived from a depleted asthenospheric mantle source (Dash et al., 2015). Chinese Jianguo basalts from Fuxin, Liaoning Province, are also of a similar age to Tsost Magmatic Field basalts and Dych Gol lavas ($^{40}Ar/^{39}Ar$; 104 Ma ± 1.6 Ma), have similar isotopic signatures ($^{87}Sr/^{86}Sr_{(i)} = 0.7034–0.704$ and $^{143}Nd/^{144}Nd_{(i)} = 0.5127$) and have been interpreted to be derived from a depleted asthenospheric mantle source (Zhang and Zheng, 2003). Asthenospheric lavas from the Basin-and-Range (USA) and Turkey (Anatolia) also have compositions similar to Tsost Magmatic Field basalts (Fig. 8A). Thus, Tsost Magmatic Field basalts have Sr and

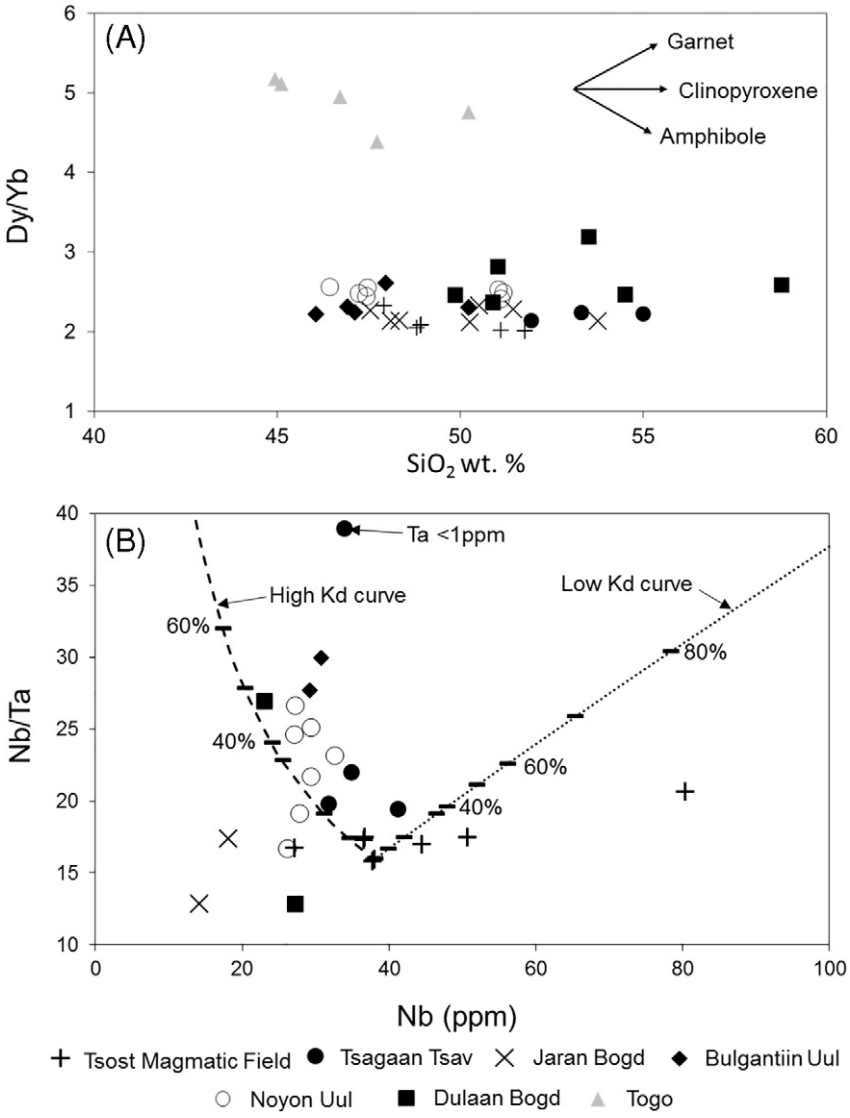

Fig. 7. (A) Dy/Yb vs. SiO_2 wt% plot with the Gobi samples and also the Cenozoic Togo basalts from Mongolia plotted (Barry et al., 2003; Davidson et al., 2012). (B) A Nb/Ta vs. Nb plot showing results of Rayleigh fractional crystallization modelling for ilmenite and spinel using sample TB95–6.3 from Tsost Magmatic Field as the starting composition. The partition coefficients used are those compiled from Klemme et al. (2006). Tick marks are in 10% fractionation intervals.

Nd isotopic signatures that suggest derivation from a depleted asthenospheric mantle source.

In contrast, the Tsagaan Tsav sample (TB95-8.2) has a higher $^{87}Sr/^{86}Sr_{(i)}$ and lower $^{143}Nd/^{144}Nd_{(i)}$ isotopic value (0.7053 and 0.5125 respectively; $\varepsilon_{Nd(t)} = 0.92$) than Tsost Magmatic Field samples, and plots within the field of the other Mongolian Mesozoic lavas that were analyzed by Dash et al. (2015). These samples form an array that extends from the field of asthenosphere-derived melts towards lithosphere-derived lavas from China, Basin-and-Range (USA) and Turkey (Fig. 8A).

Tsost Magmatic Field basalts have $^{207}Pb/^{206}Pb_{(i)}$ vs. $^{206}Pb/^{204}Pb_{(i)}$ values that are close to the NHRL (Northern Hemisphere Reference Line) and are similar to the "Chinese Mesozoic asthenospheric melts field" (Fig. 8B). As discussed by Zhang and Zheng (2003), these Chinese Mesozoic basalts, and by extension the Tsost Magmatic Field basalts, have Pb isotopic values that are more similar to MORB rather than OIB. Tsost Magmatic Field samples therefore have Pb isotopic values that support a depleted asthenospheric mantle as the source. The Tsagaan Tsav sample plots above the NHRL, in the "north-eastern and south-eastern (USA) lithospheric melts transition zone" field; thus, Tsagaan Tsav has Pb isotopic signatures consistent with a lithospheric mantle source. However, we can't rule out the possibility of crustal contamination on this data alone.

The lack of mantle xenoliths and the evolved nature of the lavas suggest magma ascent was unlikely to have been rapid. Instead, the magmas probably evolved in crustal magma chambers, where there was opportunity for crustal assimilation. The presence of granulite crustal xenoliths in samples from Tsagaan Tsav and Tsost Magmatic Field, supports the idea that crustal contamination processes occurred to some extent.

To assess whether crustal contamination of an asthenospheric melt like Tsost Magmatic Field could produce the isotopic lithospheric signature of the Tsagaan Tsav sample, AFC modelling results are presented (Fig. 8A & B), using the equations from DePaolo (1981). Sample TB95-6.3.5 from Tsost Magmatic Field is used as the initial magma due to its high MgO content; at 7.98 wt% it is one of the least evolved samples in the suite. A granulite crustal xenolith (TB95-2.5) from the Gobi Altai (Barry et al., 2003) is used as the contaminant, because of its low Nd, and high Sr and Pb isotopic values.

Assuming an r-value ("r" = assimilation against fractionation rate) of 0.3, approximately 50% of the magma would have to crystallise (i.e. F = 0.5, where "F" = mass of magma/initial mass of magma) to get

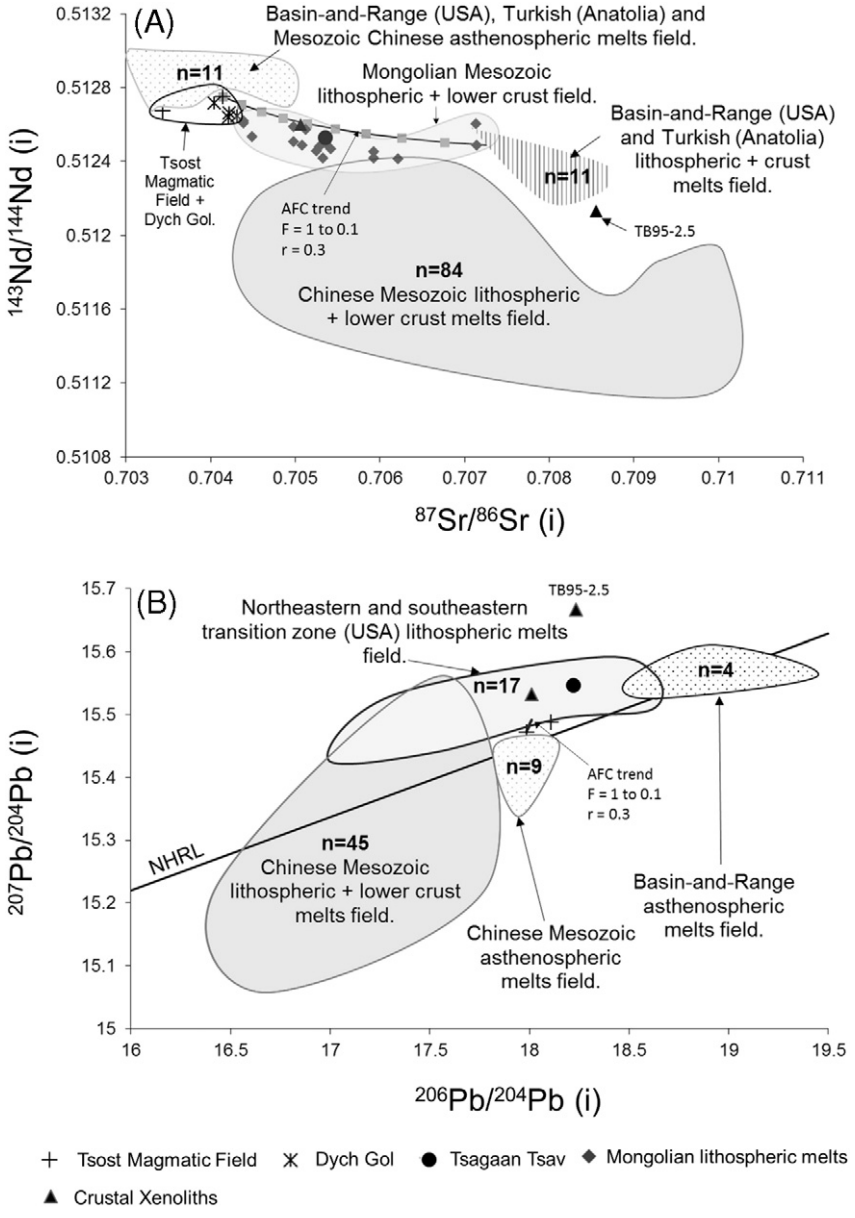

Fig. 8. (A) Plot of $^{143}Nd/^{144}Nd_{(i)}$ vs. $^{87}Sr/^{86}Sr_{(i)}$ and (B) a $^{207}Pb/^{204}Pb_{(i)}$ vs. $^{206}Pb/^{204}Pb_{(i)}$ plot for the Gobi samples. Other Mongolian samples from Dash et al. (2015); Chinese lavas (Fan et al., 2004; Gao et al., 2008; Hong-Fu et al., 2004; Zhang et al., 2002, 2004); Basin-and-Range, USA (Kempton et al., 1991 and Bradshaw et al., 1993; Pb isotope data non-age corrected) and Turkey, Anatolia (Aldanmaz et al., 2000). AFC trend uses a r value of 0.3 and a D value of 1.2 for Sr and 0.2 for Pb. The amount of F ranges from 1 to 0.1 and tick marks are in 10% intervals. The contaminant (TB95–2.5) and other granulite crustal xenoliths are from Barry et al. (2003) and are age corrected to 107 Ma.

$Sr_{(i)}$ and $Nd_{(i)}$ values close to the Tsagaan Tsav sample. Furthermore, to explain some of the other Mongolian lavas analyzed by Dash et al. (2015) with this contaminant would require F-values >0.8 (Fig. 8A; Mongolian Mesozoic lithospheric + lower crust field). Because the granulite contaminant is low in Pb (0.7 ppm), even when F-values > 0.9, AFC processes with this contaminant could not explain the Pb isotopic composition of the Tsagaan Tsav sample (Fig. 8B). Thus, it seems unlikely that AFC processes can account for the difference in isotopic signature between Tsagaan Tsav and Tsost Magmatic Field samples based on known granulite compositions.

An alternative approach to assessing the role of crustal contamination is to consider Nb/La ratios. Given that the partition coefficients for Nb and La are not significantly different for olivine, pyroxene and plagioclase (McKenzie and O'nions, 1991), the Nb/La ratios should not change significantly as a result of fractional crystallization. We can, therefore use a relatively straightforward mass balance approach to consider crustal contamination. This analysis allows us to consider different theoretical parental magmas (and contaminants), to test whether increasing assimilation of the continental crust can explain the negative Nb/La anomaly observed in all the lavas (Fig. 9). We use the equation:

$$Ca = \frac{(Cp \times 100) + (CC \times \%volume\ assimilated)}{(100 + \%volume\ of\ CC\ assimilated)}$$

where *Ca* is the composition of the lava after assimilation, *Cp* is the composition of the parental lava and *CC* is the composition of the contaminant. This equation shows that when 100% volume of *CC* is assimilated (a total volume increase to 200%) it would dilute/enrich *Cp* by 50%, or if 300% volume of *CC* is assimilated (a total volume increase to 400%) it would dilute/enrich *Cp* by 75% with respect to *CC*, highlighting the amount of assimilation required to get compositions close to *CC*.

To calculate how much crustal contamination would be required to explain the negative Nb/La ratios, an average OIB composition from

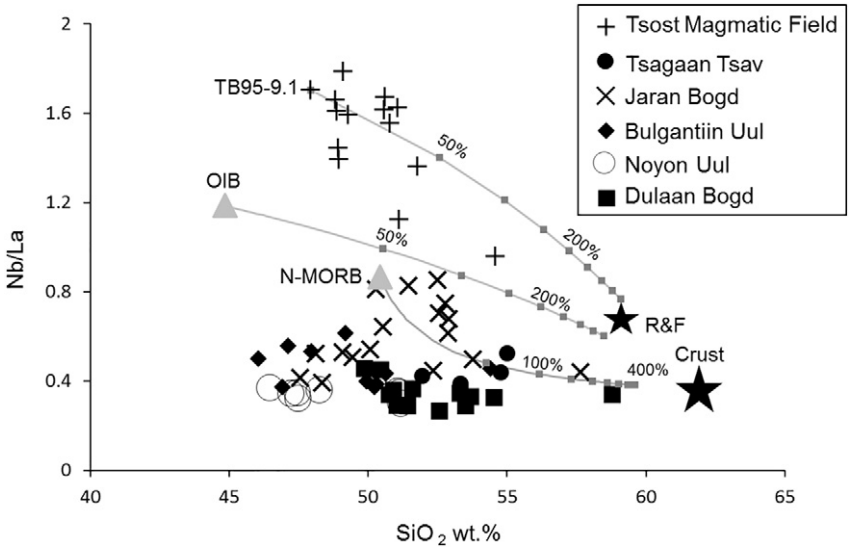

Fig. 9. (A) A Nb/La vs. SiO_2 wt% plot for the different magmatic fields showing different theoretical parental magmas which are undergoing assimilation of the crust. Parental magmas are; an average OIB (Fitton et al., 1991) and an N-MORB from Gale et al. (2013). Curves show assimilation; tick marks are shown on the curves which represent the amount of assimilation of the crust (CC), and are in 50% volume increments. The continental crust value was taken from Gao et al. (1998) and represents the interior of the North China Craton and was calculated on a carbonate rock-free basis. The average continental crust (RF) from Rudnick and Fountain (1995) is also plotted.

Fitton et al. (1991) is used to represent a Nb-rich parental magma. The crustal contaminant is a representative of the upper and lower crust from the interior of the North China Craton and was calculated on a carbonate rock-free basis (Gao et al., 1998). The average continental crust from Rudnick and Fountain (1995) is also plotted, but not used in the model due to the Nb/La ratios being higher than most of the lavas and as such could not explain the lavas' low ratios. The model suggests that to get low Nb/La concentrations purely by crustal contamination, using an OIB parental magma, would require significant amounts of assimilation. Even after 400% volume of the *CC* is assimilated the Nb/La ratios of the *Ca* are still higher (~0.6) than most of the Gobi lavas and it now has a SiO_2 content >58 wt% (silica-saturated). In this model, the OIB parental magma would require lower starting SiO_2 compositions coupled with large amounts of assimilation to be able to explain the low Nb/La ratios of the Gobi lavas and thus seems unlikely.

In summary, although it seems unlikely that the Mongolian lavas could have traversed through the continental crust without undergoing some crustal contamination, based on the analysis above, it appears that consequences of that contamination are relatively small compared with the effects of compositional variation in the source. We consider this more fully in the following section.

7. Source and melting conditions

7.1. A changing source

Since the negative Nb anomaly in the lavas likely reflects a source or mineral control, a Ta/Yb vs. Th/Yb diagram can be used to investigate source characteristics (Pearce, 1983). The ratios of these elements are largely unaffected by partial melting and fractional crystallization when pyroxenes or feldspars are the dominant crystallizing or residual phases (e.g., Irwin, 2006). The volcanic plugs from Tsost Magmatic Field plot within the mantle array (Fig. 10); melts that normally plot here are those from the asthenosphere, non-plume or plume-related asthenosphere, or from mantle lithosphere that has been enriched by melts from the asthenosphere. Enrichment in Th, with respect to Ta, will displace samples vertically on this diagram. Such an enrichment may result from source region metasomatism caused by subduction components preferentially carrying Th, over Ta and Yb. Crustal contamination may also displace samples vertically if the contaminant has abundant Th. The average upper and lower crust from Rudnick and Fountain (1995) plot outside the mantle array. The lower crust has notably lower Th/Yb ratios due to being dominantly granulite facies. This plot therefore supports the interpretation that Tsost Magmatic Field basalts have not undergone significant crustal contamination and suggests they have not come from a mantle source that has undergone significant subduction modification processes. The melts also have higher Ta/Yb and Th/Yb ratios than N-MORB, closer to OIB, suggesting the melts originated from either a garnet-bearing source, with low degrees of partial melting, or from mantle that has been enriched by asthenospheric melts, or a combination of the two. It can be seen that the Gobi lavas are displaced vertically from the mantle array towards higher Th/Yb ratios, suggesting there may be a subduction component involved in their source. The Th/Yb ratios don't show a relationship with SiO_2, other than perhaps melts from Jaran Bogd, indicating that these ratios have not been influenced by late stage crustal contamination or fractionation (see inset diagram on Fig. 10), and even samples with low SiO_2, such as those from Noyon Uul and Bulgantiin Uul (~46 wt%), don't plot within the Ta/Yb – Th/Yb mantle array. The low comparative Ta abundances in the lavas, as shown on primitive mantle normalization diagrams (Fig. 6), is largely responsible for these lavas not plotting in the mantle array. The mantle source was therefore depleted in Ta (and Nb). Metasomatism of the lithosphere, caused by the release of fluids during previous subduction events could have created lithospheric pockets which are enriched in the LILE while also being depleted in Nb and Ta. Therefore the depletion in Nb, Ta and enrichment of the LILE indicates a source which has been conditioned by previous subduction events.

Basanite lavas from the Dych Gol area of eastern Mongolia (Dash et al., 2015) are also plotted, as these plot in the mantle array and are similar in age to the Tsost Magmatic Field basalts. For comparison with areas that have undergone thickening and then extension, lavas from the southern Basin-and-Range, USA (Bradshaw et al., 1993) and from western Anatolia, Turkey (Aldanmaz et al., 2000) are also plotted on the Ta/Yb vs. Th/Yb diagram (Fig. 10). The oldest lavas from both areas have lithospheric mantle signatures that plot outside the mantle array, while the younger lavas plot within the mantle array; similar to the Mesozoic melts from the Gobi.

Interestingly, the switch from lithospheric-dominated magmatism to asthenospheric-dominated magmatism seems to have happened at a similar time in both Mongolia and China, as shown in Fig. 11. Rocks older than 107 Ma have relatively low Nb/La values (average of 0.34 ± 0.17), whereas younger basalts have significantly higher ratios (average

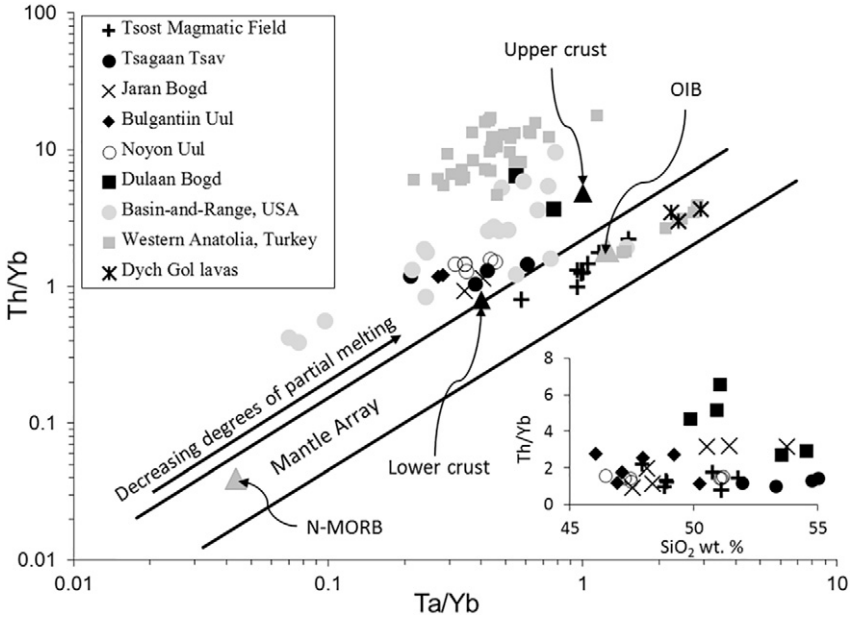

Fig. 10. Ta/Yb vs. Th/Yb diagram of Pearce (1983) showing Gobi samples, Dych Gol lavas, lavas from the Basin-and-Range USA and from Western Anatolia, Turkey (Aldanmaz et al., 2000; Bradshaw et al., 1993 and Dash et al., 2015). Also plotted is an OIB from Sun and McDonough (1989) and average N-MORB from Gale et al. (2013).

of 1.42 ± 0.23). These younger basalts are either interpreted to be asthenospheric melts or newly replaced lithospheric melts. However, the locations of the asthenospheric-dominated magmatism occur large distances from each other. For example, the Mesozoic Jianguo basalts from Fuxin, Liaoning Province (China), despite being a similar age to Tsost Magmatic Field basalts, are approximately ~1600 km away from the Gobi Altai. Similarly, the asthenospheric Mongolian Dych Gol lavas are approximately ~1150 km away from Tsost Magmatic Field. This would imply that the magmatism is linked to some large-scale process.

To further consider magmatic/metasomatic processes that may have affected the lithospheric mantle source, a Zn/Fe ratio plot is utilized to consider source characteristics (Fig. 12A). High Zn/Fe ratios have been used to identify pyroxenite source lithology, or garnet-pyroxene-rich sources that generate high Zn/Fe ratios by fractionation during partial melting (Le Roux et al., 2010; a pyroxenite source can generate Zn/Fe values as high as ~14, at 12 MgO wt%, or even higher values if the source is garnet-rich). This is because Zn and Fe partition equally between olivine and orthopyroxene under mantle conditions ($K^{\frac{Zn}{Fe}}_{D\,(\frac{Ol}{melt})} \sim K^{\frac{Zn}{Fe}}_{D\,(\frac{Opx}{melt})} = \sim 0.9-1$), whereas Zn is more incompatible than Fe in garnet and clinopyroxene ($K^{\frac{Zn}{Fe}}_{D\,(\frac{Cpx}{melt})} \sim K^{\frac{Zn}{Fe}}_{D\,(\frac{Gt}{melt})} = <1$). However, high Zn/Fe melts can be produced from a peridotite source if metasomatism has enriched it in Zn (Le Roux et al., 2011). Therefore Zn/Fe ratios are not necessarily a sensitive indicator of non-peridotite source lithology (Davis et al., 2013) but may be an indication of source region metasomatism; thus Fig. 12 shows source variation rather than source rock identification.

Although all the Gobi volcanic provinces have undergone clinopyroxene fractionation which will mask some aspects of source geochemistry and metasomatic processes, the plot clearly shows that Tsost Magmatic Field basalts have lower Zn/Fe ratios than the Gobi

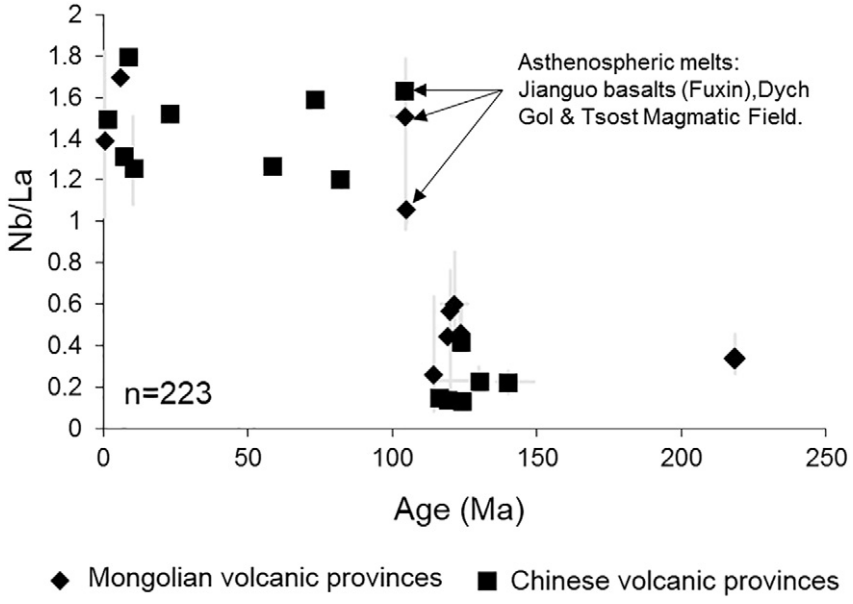

Fig. 11. Nb/La vs. Time (Ma) plot, showing the average values for different volcanic provinces across Mongolia ($n = 113$ samples: Barry et al., 2003; Dash et al., 2015 and this study) and China ($n = 110$ samples; Zhang et al., 2002; Zhang and Zheng, 2003; Liu et al., 2008 and reference therein); bars show the minimum and maximum values for each volcanic province.

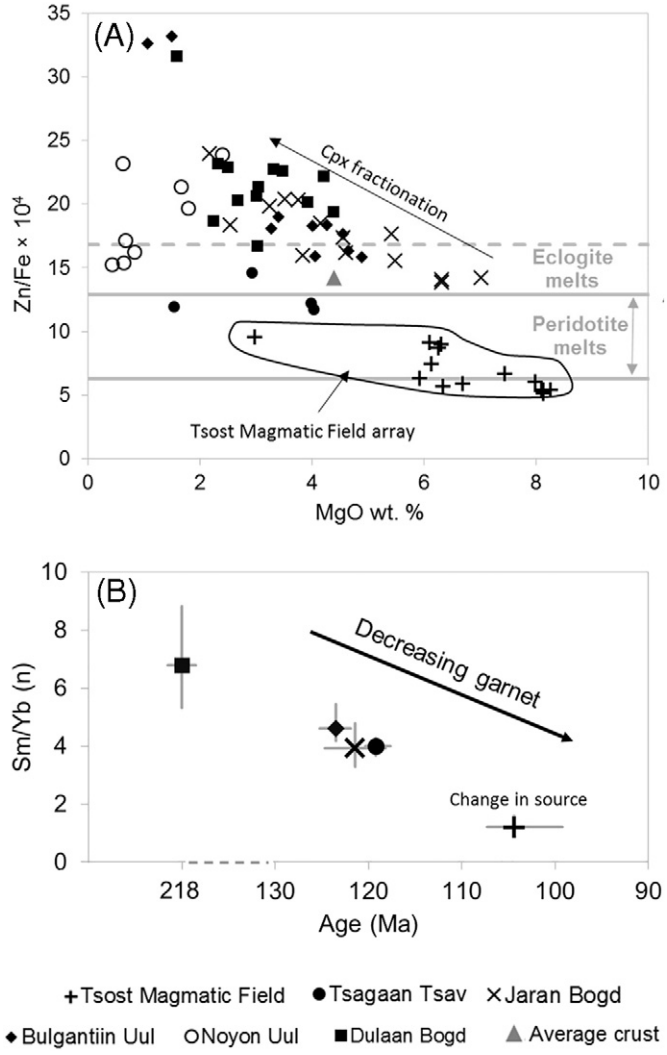

Fig. 12. (A) Zn/Fe ($\times 10^4$) ratios vs. MgO wt% plot ($FeO = \left(\frac{Fe_2O_{3(T)}}{(1+(\frac{0.2}{111}))}\right)/1.111$). The peridotite melts field and the upper eclogite field is based on information in Le Roux et al. (2010), however evolved samples which have undergone clinopyroxene fractionation will plot outside this field. Average crust value was taken from Rudnick and Fountain (1995). (B) Average primitive mantle-normalized Sm/Yb ratios (Sun and McDonough, 1989) vs. age for each magmatic field. Bars show the minimum and maximum range for each magmatic field.

Altai lavas. The higher Zn/Fe ratios for the Gobi lavas relative to Tsost Magmatic Field is consistent with fractionation processes and/or source metasomatism and potentially a different source lithology.

Interestingly, average Zn/Fe ratios from each magmatic field decreases with decreasing age: 21.77 for Dulaan Bogd; 20.53 for Bulgantiin Uul; 17.60 for Jaran Bogd, 12.64 for Tsagaan Tsav and 5.79 for Tsost Magmatic Field. Furthermore, if we only consider averages from samples with between 4 and 5 wt% MgO (most volcanic provinces have <5 wt% MgO) to try and remove fractionation bias, average Zn/Fe ratios still generally decrease with age: 20.81 for Dulaan Bogd; 17.03 for Bulgantiin Uul; 17.36 for Jaran Bogd and 11.79 for Tsagaan Tsav. The highest Zn/Fe ratio from Tsost Magmatic field is 9.57 and that is from a sample (TB95–9.5.2) with 2.98 wt% MgO; thus Tsost Magmatic Field rocks must have the lowest Zn/Fe ratios for a given MgO. This could suggest that any involvement from a metasomatised source could have had decreasing input with time and/or perhaps there was less involvement from garnet in the source too. Alternatively, there could have been less involvement from a hybridized source, such as peridotite + eclogite/pyroxenite.

To further evaluate geochemical changes with time, for the Gobi magmatic provinces, consideration is now given to garnet controls. Low chondrite-normalized Dy_n/Yb_n ratios (often <1.8) characterize melts which are derived from a spinel lherzolite source (e.g., Blundy et al., 1998) but all the Gobi samples have ratios >2, suggesting that garnet was involved. We consider the change in garnet signature through time using Sm/Yb ratios. We use this ratio because Yb is highly compatible in garnet but not clinopyroxene. Primitive mantle-normalized Sm_n/Yb_n ratios are compared for each of the Gobi magmatic fields (Fig. 12B); the decreasing Sm_n/Yb_n ratios with time suggest diminishing garnet involvement for magmatic fields on the Gobi Altai terrane. One explanation for this reduced garnet signature is that there was less involvement from a garnet-bearing source and/or increased decompression melting in the spinel peridotite facies with time.

7.2. Peridotite vs. pyroxenite source: geochemical indicators

From a petrological perspective, peridotite and pyroxenite are distinguished lithologically on the basis of mineral proportions of pyroxene versus olivine: peridotite, by definition, consists of >40% olivine while pyroxenite has <40% olivine. Factors such as temperature, pressure and other mineral phases (e.g., spinel, garnet, Fe-Ti oxides) will influence the relative proportions of olivine and pyroxene.

Distinguishing peridotite from pyroxenite sources on the basis of lava composition can thus be difficult. Furthermore, processes such as magma mixing, fractional crystallization and metasomatism can affect the final lava composition and, hence, obscure geochemical signals indicative of different source types. However, the involvement of pyroxenite as either a source rock, or as an addition (e.g., pyroxenite veins in the source rock), in magma genesis makes for an interesting debate (e.g., Yang et al., 2016; Yang and Zhou, 2013). Pyroxenite has been suggested as the source rock for Chinese Cenozoic basalts, while pyroxenite veins hosted in a peridotite source have been suggested for Mesozoic Chinese lavas (Liu et al., 2008; Yang et al., 2016).

Whole-rock CaO-MgO relationships have been used to distinguish peridotite from pyroxenite sources (Herzberg, 2006), because melts derived from peridotite should theoretically have higher CaO contents at a given MgO wt%. However, as emphasised in the appendix of Herzberg (2006), for alkali melts, peridotite melting can produce low-CaO melts. Furthermore, studies have shown that metasomatised garnet peridotite and small degree melts derived from a MORB-eclogite source that has interacted with peridotite on its way to the surface, can produce low-CaO basaltic melts at garnet-stable pressures (Mallik and Dasgupta, 2012). Therefore, as peridotite sources are capable of producing both low and high CaO melts, this scheme is unsuitable for determining source characteristics for the Mongolian lavas and thus not considered further.

Olivine phenocryst composition has been used to distinguish peridotite from pyroxenite source lithology (e.g., Herzberg et al., 2014). Olivine in basalts, which has low Ca and Mn, with high Ni and high Fe/Mn ratios at a given Fo content are features associated with a pyroxenite source. However, recognising whether olivine phenocrysts are xenocrysts can be difficult. Furthermore, olivine commonly exhibits chemical zoning; these zones can exhibit geochemical variance, which may lead to wrong interpretations. This is particularly important when considering the Gobi samples, as olivine is nearly always altered partially or completely to iddingsite. Therefore, finding and probing exposed areas of fresh olivine phenocryst can be difficult and may not truly represent the original mineral. Furthermore, it has been shown that temperature can have a significant influence on how Ni partitions between olivine and the melt (e.g., Matzen et al., 2013), and therefore source/melt composition is not always the only control.

Based on melting experiments on peridotite and pyroxenite, a FC3MS (FeO_T/CaO-3 × MgO/SiO_2 wt%) parameter was generated to distinguish peridotite from pyroxenite sources (Yang and Zhou, 2013). This parameter is primarily controlled by source composition and

melting degree, while pressure and temperature have little effect. Fractionation controls also occur, with clinopyroxene fractionation increasing FC3MS values.

High FC3MS results are typically attributed to a pyroxenite source. To try and account for fractionation of the evolved Gobi melts, corrections have been applied to the oxides. However, the uncorrected data are plotted for comparison (Fig. 13). The correction on the oxides utilizes the equation given in the appendix of Niu and O'Hara (2007). All the Gobi data are corrected to a Mg-number of 72. However, correcting a highly evolved melt back to a Mg-number of 72 is difficult and prone to error. Lavas with <1.5% MgO wt% were not included in the correction procedure. Although alteration may have affected the major elements, LOI values are mostly <2 wt% (although samples from Noyon Uul range from 2.29–4.49 wt%) and the clear relationship between FC3MS values and MgO suggests that fractionation is the dominant control on these values.

A polynomial equation was utilized on MORB (Niu et al., 1999) to determine the polynomial coefficients (m_n). Using these polynomial coefficients the Gobi data have been corrected using the equation:

$$Y^{72} = Y_{Data} + \sum_{n-1}^{N} M_n \left(X_{72}^n - X_{Data}^n\right)$$

where n refers to the n^{th} term of the polynomial equation.

For comparison purposes, experimental peridotite and pyroxenite melts are plotted. Also plotted are Cenozoic basalts from China that have been interpreted as pyroxenite melts (uncorrected for fractionation) and are discussed in detail by Yang et al. (2016). Cenozoic basalts from the Tariat-Chuloot Formation are plotted (as both uncorrected values and values corrected for fractionation); these rocks have been interpreted as peridotite melts (Barry et al., 2003), or possibly garnet-pyroxenite melts (Hunt, 2011). Pleistocene and Quaternary Mongolian basalts from Orkhon and Togo (Hunt et al., 2012) are also plotted (uncorrected for fractionation) and previous trace-element interpretations define these as originating from a pyroxenite source, with the Togo basalts also being derived from amphibole-rich regions of the mantle (Barry et al., 2003; Hunt, 2011).

The Chinese Cenozoic basalts have high FC3MS values at a given MgO wt%, consistent with their pyroxenite source interpretation. The Orkhon and Togo basalts have high FC3MS values (0.87–0.89 and 0.45–0.62, respectively), plotting with the Chinese Cenozoic basalts, suggesting that the Orkhon basalts originated or interacted with a pyroxenite source while the Togo basalts are more ambiguous. Modelling done by Yang and Zhou (2013) indicates that the highest FC3MS value that can be produced from peridotite melting is 0.65 when MgO is >7.5 wt%. Two Togo samples have 7.4 wt% MgO and have a FC3MS value of 0.61–0.62, which is very close to the upper limit achievable by peridotite melting. Therefore, FC3MS values for the Togo basalts are likely consistent with trace-element interpretations by Hunt (2011). The Cenozoic Tariat-Chuloot lavas have FC3MS values that are generally higher than the Mesozoic Gobi samples at comparable MgO wt%, but display a range of FC3MS values.

Many of the Cenozoic Mongolian basalts have high LREE/HREE and MREE/HREE ratios, which have been used to infer depth of melting (Barry et al., 2003). These ratios are often higher than those in the Mongolian Mesozoic samples, which could be interpreted to reflect melting at greater depth. However, if the Cenozoic basalts are primarily pyroxenite-derived products, the typical garnet signature implied by the LREE/HREE and MREE/HREE ratios might not be indicative of a high-pressure garnet source, because garnet can be stable at lower pressures in pyroxenite (e.g., Lambart et al., 2013; Yang et al., 2016 and references therein).

The Gobi samples have high FC3MS values at low MgO wt% (uncorrected for fractionation) likely due to clinopyroxene fractionation, although values are mostly lower than the Orkhon and Togo basalts. Many Gobi samples also have FC3MS values lower than the experimental pyroxenite melts and Chinese Cenozoic basalts at comparable MgO wt%. Jaran Bogd lavas display a range of FC3MS values between samples with comparable MgO wt%, perhaps indicating source variation or magma mixing. When the Gobi samples are corrected for fractionation, they plot with the peridotite experimental melts (FC3MS = 0.1–0.57);

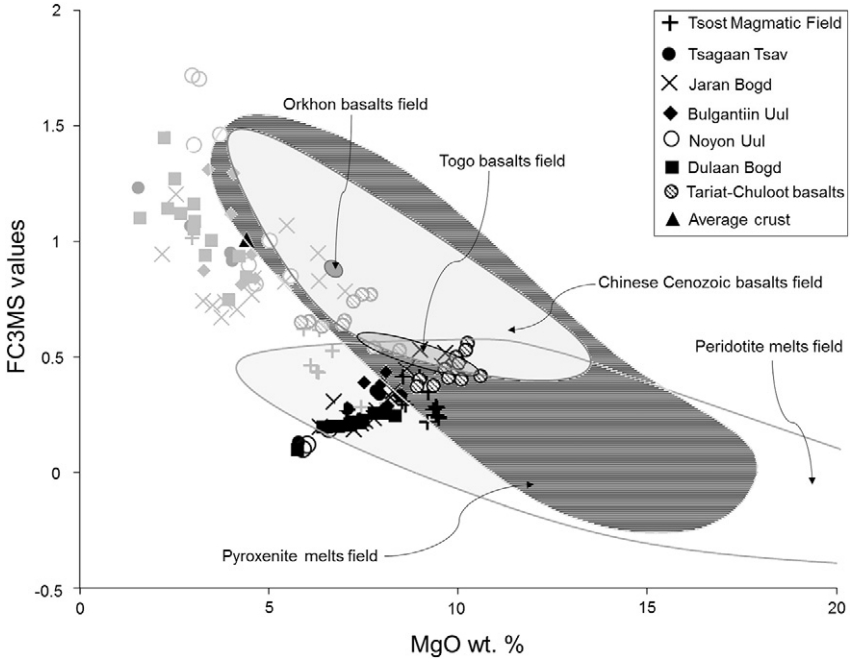

Fig. 13. FC3MS ($FeO_T/CaO-3 \times MgO/SiO_2$ wt%) values vs. MgO wt%. Fe was calculated from FeO $\left(FeO = \left(\frac{Fe_2O_{3(T)}}{(1+(\frac{0.2}{1.11T}))}\right)/1.111\right)$ for all Mongolian samples. The Chinese Cenozoic basalts are believed to be pyroxenite melts (Yang et al., 2016 and references therein). Pyroxenite and peridotite melting field is constructed from melting experiments and is from Yang et al. (2016). Orkhon and Togo Mongolian Cenozoic lavas from Barry et al. (2003). Average crust from Rudnick and Fountain (1995). The uncorrected Mongolian samples are the grey symbols. Fractionation-corrected (Mg-number of 72) FCSMS and MgO wt% values are the black symbols.

although we stress that there is much uncertainty in the correction procedure. Because so many of the Gobi samples have fractionation uncorrected FC3MS values that don't plot in the pyroxenite field, we interpret this to be because peridotite is the dominant source lithology (but it could be a combined peridotite + pyroxenite source).

7.3. Mixing between lithospheric and asthenospheric mantle melts

If the lithosphere was thinned or removed under Mongolia in the Mesozoic, as suggested for Archaean lithosphere under the North China Craton at this time (e.g., Menzies et al., 1993), and as suggested by the dramatic change in Nb/La ratio at about 107 Ma (Fig. 11), it's possible that the asthenospheric mantle had greater input to magma genesis over time. This might have been accentuated if melting happened at the base of the lithosphere, triggered in part by localized asthenospheric upwelling.

The lavas from Jaran Bogd show the greatest variation on the geochemical plots within any given province and therefore provide us with the best chance to test whether there could have been a transitional shift from a lithospheric to an asthenospheric source. Additionally, petrological studies identified subophitic clinopyroxene enclosing plagioclase feldspar and convolute zoning in feldspar phenocrysts which might be indicative of magma mixing. Furthermore, because the exposures at Jaran Bogd provide us with a stratigraphic sequence of lava flows, we have an opportunity to investigate changes in the amount of asthenospheric input with time, as we move up sequence (JB1 towards the base while JB94 is towards the top of the sequence).

Using a combination of the oxides (FC3MS values; uncorrected for fractionation) and HFSE (Nb/La and Zr), geochemical trends are used to recognize asthenospheric vs. lithospheric inputs (Fig. 14). Using the sample with the lowest SiO_2 (47.5 wt%) and high MgO (6.3 wt%) from Jaran Bogd (JB8), two trends can be recognized. Some of the lavas from Jaran Bogd have geochemical signatures more similar to the older lithospheric melts (JB1 to JB17). However, as the SiO_2 content or Nb/La ratios increase, many of the Jaran Bogd lavas trend towards Tsost Magmatic Field compositions. Interestingly, Jaran Bogd lavas have lower Zr concentrations than the other Gobi lavas, on average, and are comparable to the asthenospheric basalts from Tsost Magmatic Field. Jaran Bogd and Tsost Magmatic Field samples both have decreasing Zr with increasing SiO_2 content, perhaps indicating a mineral fractionation control, too. This suggests Jaran Bogd lavas may represent a melt from a lithospheric source with variable amounts of evolved asthenospheric input, explaining the geochemical variation observed in the lavas.

The Tsagaan Tsav lavas show a strong lithospheric mantle geochemical signature despite overlapping the dated Jaran Bogd lavas in age, i.e. 120.3 to 117.6 ± 0.3 Ma for Tsagaan Tsav lavas vs. 124.7 to 118.2 ± 1.4 Ma for Jaran Bogd. This implies that the Jaran Bogd melts may have been triggered during a greater input of asthenospheric activity or maybe some of the Jaran Bogd lavas are actually younger than the Tsagaan Tsav lavas. The youngest dated sample from Jaran Bogd (JB26) has relatively low Zr concentrations while also having a high Nb/La ratio > 0.73 compared to the other Gobi lavas. Samples JB38, JB46, JB57, JB69 and JB94 all appear stratigraphically higher in the sequence than the dated JB26 sample and show some of the greatest affinities to asthenospheric melts (relatively low Zr and Nb/La ratios ranging from 0.67 to 0.85).

8. Discussion

The Gobi lavas are depleted in some HFSE (Nb, Ta and Ti) but are enriched in Zr, the LREEs and LILEs (Fig. 6). The Tsagaan Tsav sample (Fig. 8) has relatively high $^{87}Sr/^{86}Sr_{(i)}$ and low isotopic $^{143}Nd/^{144}Nd_{(i)}$ values that are similar to other Mongolian Mesozoic SCLM derived melts (Dash et al., 2015). The Tsagaan Tsav $Pb_{(i)}$ isotope ratios are higher than the NHRL, but similar to basalts from the transition zone between

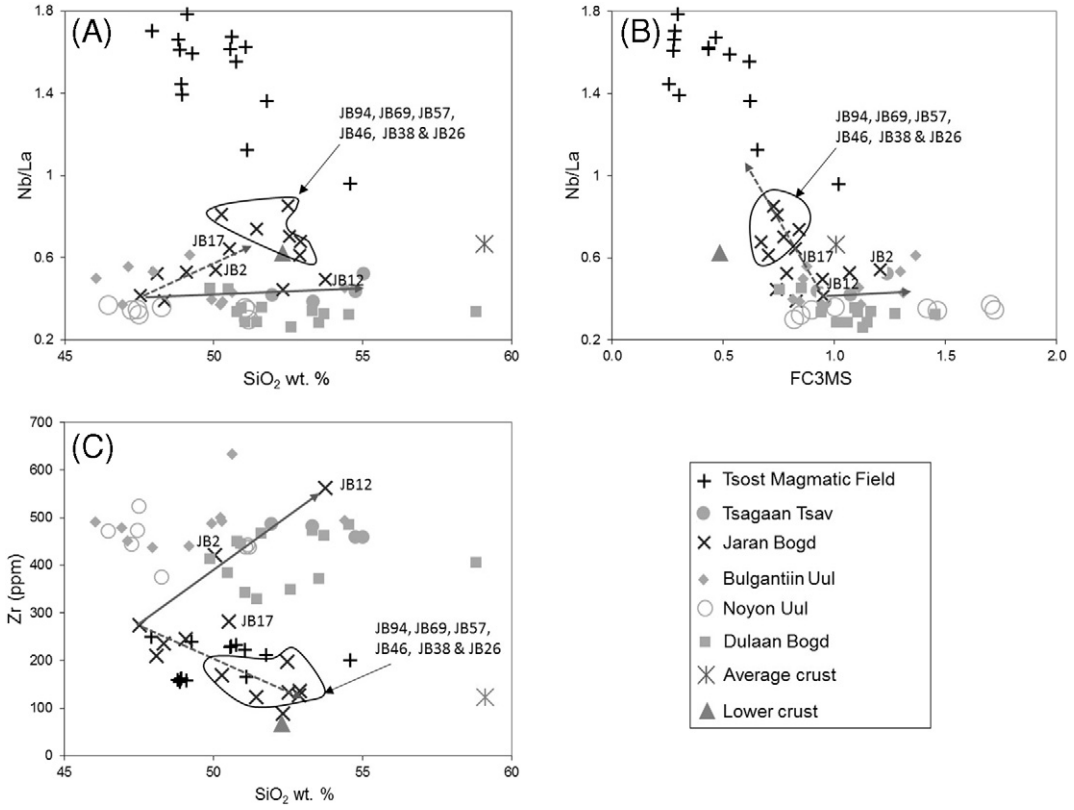

Fig. 14. Variation diagrams for the Gobi lavas showing: (A) Nb/La vs. SiO_2 wt%; (B) Nb/La vs. FC3MS (FeO_T/CaO-3 × MgO/SiO_2 wt%) values and (C) Zr vs. SiO_2 wt%. The arrows commence from sample JB8 and point in the general direction of two trends for the Jaran Bogd lavas.

the Basin-and-Range and the Colorado Plateau (USA). The Gobi lavas plot outside the mantle array on a Th/Yb vs. Ta/Yb plot and have higher Zn/Fe ratios than Tsost Magmatic Field basalts (Figs. 10 & 12A). Therefore, taken together, these data are interpreted as evidence that the Gobi lavas were derived from a metasomatised lithospheric mantle that may have been modified by melts derived from recycled rutile-bearing eclogite.

Tsost Magmatic Field basalts have low $^{87}Sr/^{86}Sr_{(i)}$, relatively high isotopic $^{143}Nd/^{144}Nd_{(i)}$ values, and $Pb_{(i)}$ isotope ratios that are close to the NHRL. Furthermore, these basalts are not depleted in the HFSE (Nb, Ta, Ti), are less enriched in Zr compared to most of the Gobi lavas (Fig. 14C), but are enriched in the LREEs and LILEs. The basalts show geochemical parallels (Figs. 8 & 11) to similar age Mesozoic basalts from Dych Gol (Mongolia) and Chinese Jianguo basalts (Fuxin, Liaoning Province). The geochemical data suggest that Tsost Magmatic Field basalts were derived from asthenospheric mantle.

Combining all this evidence (e.g. the decrease in garnet signature (Sm/Yb ratios) and magmatic/metasomatic input (Zn/Fe ratios) with time (Fig. 12), the gradual increase in asthenospheric input (Fig. 14) and a switch from lithospheric to asthenospheric magmatism) suggests that lithospheric mantle was stripped away under the Gobi. This event appears to have occurred after the Tsagaan Tsav magmatism (~118 Ma) but prior to the Tsost Magmatic Field magmatism (~107 Ma).

At the time of their eruption, the oldest dated Gobi lavas from Dulaan Bogd (~218.5 Ma), were ~150–200 km south of a subduction plate boundary associated with the closing Mongol-Okhotsk Ocean, and likely in an overriding plate position (e.g., Van der Voo et al., 2015). The Dulaan Bogd lavas are thought to have been deposited in a half-graben (Van Hinsbergen et al., 2015), and contemporaneous extensional basins were also recognized elsewhere in the Gobi Altai region (Johnson et al., 2015). Samples from all the magmatic fields are alkaline and enriched in the incompatible elements, such as Zr (88–633 ppm); thus, these volcanic rocks are not thought to be volcanic arc related.

Earlier, in the Palaeozoic, Northeast China and Mongolia amalgamated during the subduction of the Paleo-Asian Oceans and the formation of the CAOB (Xiao et al., 2015). It is therefore likely that the lithospheric mantle beneath the region had been enriched, by subduction-derived fluids and partial melts long prior to formation of the magmatic rocks studied in this paper. The presence of small amounts of water and carbon dioxide in the lithospheric mantle may have assisted partial melting by reducing the mantle potential temperature required to initiate melting.

What triggered the magmatism in the Gobi Altai region is enigmatic (e.g., Dash et al., 2015; Fan et al., 2003; He, 2015; Meng, 2003; Wang et al., 2006; Yarmolyuk and Kovalenko, 2001). Although the Mesozoic magmatism occurred over a large area, no evidence of a mantle plume has been documented. Therefore, many studies have proposed a form of delamination to account for the magmatism across the CAOB. However, the suggestion by Wang et al. (2006) that westward delamination of an earlier thickened lithospheric mantle created by the latest Jurassic-earliest Cretaceous closure of the Mongol-Okhotsk Ocean does not seem an appropriate mechanism for the genesis of the Gobi magmatic provinces due to the spread of ages within the same region and across China, and the absence of major regional shortening in Siberia or Mongolia during the latest Jurassic-earliest Cretaceous (Figs. 1B & 11).

A model of convective mantle lithosphere removal was postulated by He (2014) to explain the Mesozoic magmatism in the North China Craton. In this model, to explain the most abundant volcanism (135–115 Ma), the formation of an extensive mantle wedge is required, due to a stagnating Pacific plate beneath the North China Craton. Slab dehydration would then reduce the viscosity of the asthenosphere, and may result in small-scale upwellings within the upper mantle and convection of the mantle wedge. As the asthenosphere ascends, it may cause compression of the rheological boundary layer and consequently increases the temperature gradient within this layer. This convection and excess heat causes lithospheric thinning. The lowering of melting temperature by peridotite-melt interaction can help accelerate lithospheric thinning and, when combined with convective erosion, can result in significant thinning of a cratonic lithosphere (e.g., with a mantle viscosity of 10^{18}–10^{19} Pa s and a peridotite melting temperature of 1000–1100 °C a lithosphere could be thinned over tens of millions of years but at normal asthenospheric temperatures). In such a model, a combination of vigorous upper mantle convection, peridotite-melt interaction and local delamination results in abundant magmatism and lithospheric thinning (He, 2014, 2015).

Apart from Dulaan Bogd (and possibly Noyon Uul), the Gobi lavas erupted between 124 and 117 Ma. Thus, they were erupted over a similar time interval to the magmatism in the North China Craton. Furthermore, when we consider that asthenospheric melts appear in Mongolia and China at similar times, it suggests that the Mesozoic magmatism in the North China Craton and Mongolia are linked to a large-scale event(s) affecting the east Asian mantle lithosphere.

Given their >2000 km separation, it's not feasible that the Pacific Plate extended horizontally all the way under the Gobi region during

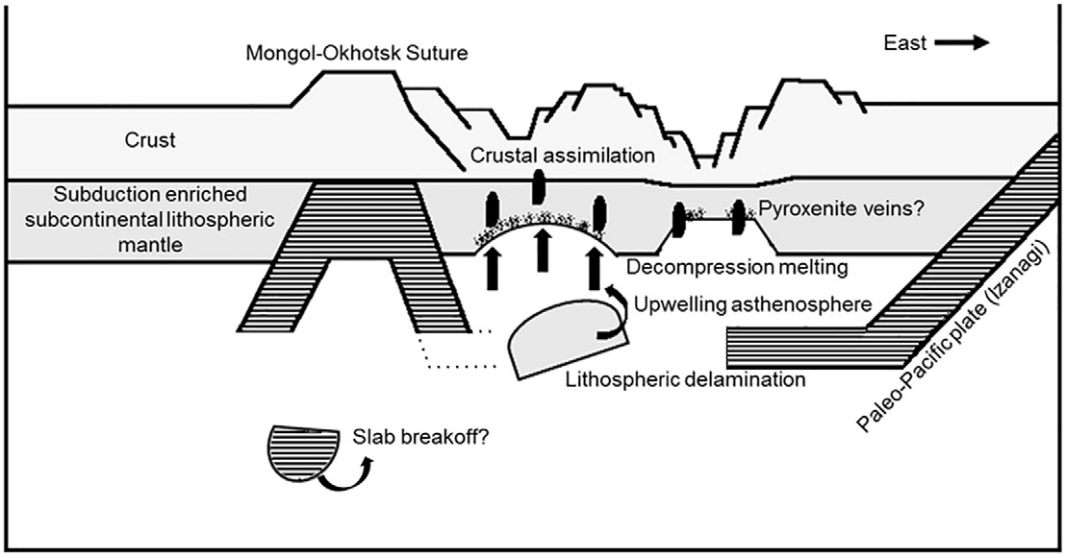

Fig. 15. An illustration showing piecemeal lithospheric delamination and decompression melting of a subduction preconditioned lithosphere after the closure of the Mongol-Okhotsk Ocean. Slab breakoff may have also aided extensional events and facilitated rising asthenospheric melts.

the Mesozoic. A southward subducting Mongol-Okhotsk slab may have extended far enough southwards to create an extensive mantle wedge below the Gobi region. It is also unclear how asthenospheric upwelling would be triggered over such a vast area so as to result in convective thinning under the Gobi region at the same time as that under the North China Craton. Therefore, we suggest that the convective model by He (2014, 2015), involving just the Pacific Plate, may not fully account for the extensive volcanism observed.

Interpreting this period of Gobi volcanism as the product of delamination, as suggested for similar age volcanism in the North China Craton (e.g., Windley et al., 2010), faces similar challenges in terms of the density contrasts between lithospheric keel and the asthenosphere (e.g., Menzies et al., 2007). That is, if a thick lithospheric keel (lower crust) was converted to eclogite, then a density contrast between the lower crust and lithospheric mantle may have assisted delamination. However, the absence of crustal eclogite xenoliths in the Gobi lavas makes it difficult to confirm this scenario.

Without further investigation into the magmatism across Mongolia it is difficult to assess whether the volcanism as a whole was a prolonged, gradual event or a relatively rapid one. If it was a rapid delamination model, it is unclear why so many places delaminated at the same time to give the asthenospheric signal, like that from Tsost Magmatic Field. Nonetheless, based on the available data, we suggest that the delamination model is the best scenario, because of the similar age volcanism in the Gobi and across eastern Mongolia (Dash et al., 2015) as that in the North China Craton.

Thus, the following model is proposed to explain the Gobi volcanism:

(1) The lithosphere under the Gobi Altai was modified by previous metasomatic events and possibly by melts derived from recycled rutile-bearing eclogite. The oldest dated lavas (218.5 Ma), from Dulaan Bogd, erupted onto a thick lithosphere. Because the lithosphere was thick it could have provided a barrier to magma reaching the surface. It is thus difficult to assess whether Dulaan Bogd magmatism is evidence of a gradual lithospheric removal processes under the Gobi region, or whether this magmatism is just unrelated to later postulated delamination processes.
(2) Because the rest of the dated Gobi lithospheric mantle melts are a similar age (~124–118 Ma) to much of the volcanism in the North China Craton (~135–115 Ma) and eastern Mongolian lithospheric mantle melts (120–114 Ma), we suggest that this favours a rapid delamination model across the whole of the region (Fig. 15). The closure of the Mongol-Okhotsk Ocean may have helped provide the necessary conditions for delamination in the Gobi.
(3) As the lithosphere was gradually stripped away, younger Mesozoic asthenospheric melts (~107 Ma) were able to erupt. However, because asthenospheric melts appear elsewhere in Mongolia and the North China Craton at a very similar time, we suggest that a period of large-scale (possibly localized) asthenospheric upwelling occurred.

9. Conclusions

(1) The Gobi lavas are LREE and LILE-enriched while being depleted in some HFSE (Nb, Ta and Ti). The Tsagaan Tsav sample has relatively high $^{87}Sr/^{86}Sr_{(i)}$ and low $\varepsilon Nd_{(i)}$ values and are comparable to other Mongolian Mesozoic lavas. $Pb_{(i)}$ isotope ratios plot above the NHRL, but are similar to basalts from the transition zone between the Basin-and-Range and Colorado Plateau (USA), consistent with an interpretation as subcontinental lithospheric mantle melts. The Gobi lavas represent melts from a subduction-preconditioned lithospheric mantle that was likely modified from recycled rutile-bearing eclogite melts and metasomatism. What triggered the melting is unclear, but delamination is a potential mechanism.
(2) The volcanic plugs from Tsost Magmatic Field are LREE- and LILE-enriched and are not depleted in the HFSE. These melts have low $^{87}Sr/^{86}Sr_{(i)}$ and relatively high $\varepsilon Nd_{(i)}$ values; $Pb_{(i)}$ isotope ratios plot close to the NHRL. The geochemical data suggest that Tsost Magmatic Field basalts were derived from the asthenospheric mantle.
(3) FC3MS values suggest that pyroxenite is not the dominant source lithology under the Gobi region. However, some of the Cenozoic lavas from Mongolia may be pyroxenite-derived melts.
(4) The decrease in garnet signature (Sm/Yb ratios), and magmatic/metasomatic input (Zn/Fe ratios) with time, the gradual increase in asthenospheric input and a switch from lithospheric to asthenospheric magmatism suggests that the lithospheric mantle was stripped away under the Gobi, with its removal by ~107 Ma.
(5) Asthenospheric melts appear in Mongolia at a similar time interval to those in China. This suggests some large-scale process was responsible for asthenospheric upwelling because distances between this asthenospheric magmatism is up to ~1600 km.

Supplementary data to this article can be found online at https://doi.org/10.1016/j.lithos.2017.11.016.

Acknowledgments

The fieldwork and analyses from T. Barry were supported by NERC studentship GT4/95/155/E, with thanks to B. Windley. We thank M. Pringle and D. Barfod for running and recalculating the Ar-Ar dating work, respectively. Thanks to S. Dempsey for collecting and analyzing the Noyon Uul samples. DJJvH acknowledges ERC Starting grant 306810 (SINK) and NWO VIDI grant 864.11.004, UK NERC Grant NER/D/S/2003/00671, funding from the Univeristy of Leicester to perform geochemical analyses, and Dickson Cunningham for the opportunity, guidance, and support in studying Mongolian geology.

References

Aldanmaz, E., Pearce, J.A., Thirlwall, M.F., Mitchell, J.G., 2000. Petrogenetic evolution of late Cenozoic, post-collision volcanism in western Anatolia, Turkey. Journal of Volcanology and Geothermal Research 102 (1), 67–95.
Badarch, G., Cunningham, W.D., Windley, B.F., 2002. A new terrane subdivision for Mongolia: implications for the Phanerozoic crustal growth of Central Asia. Journal of Asian Earth Sciences 21 (1), 87–110.
Barry, T.L., 1999. Origins of Cenozoic Basalts in Mongolia: A Chemical and Isotope Study (Doctoral dissertation, Geology).
Barry, T.L., Saunders, A.D., Kempton, P.D., Windley, B.F., Pringle, M.S., Dorjnamjaa, D., Saandar, S., 2003. Petrogenesis of Cenozoic basalts from Mongolia: evidence for the role of asthenospheric versus metasomatized lithospheric mantle sources. Journal of Petrology 44 (1), 55–91.
Bennett, S.L., Blundy, J., Elliott, T., 2004. The effect of sodium and titanium on crystal-melt partitioning of trace elements. Geochimica et Cosmochimica Acta 68 (10), 2335–2347.
Blundy, J.D., Robinson, J.A.C., Wood, B.J., 1998. Heavy REE are compatible in clinopyroxene on the spinel lherzolite solidus. Earth and Planetary Science Letters 160 (3), 493–504.
Bradshaw, T.K., Hawkesworth, C.J., Gallagher, K., 1993. Basaltic volcanism in the Southern Basin and range: no role for a mantle plume. Earth and Planetary Science Letters 116 (1–4), 45–62.
Chakraborty, K.R., 1980. On the evolution of the nepheline to hypersthene normative alkali basaltic rocks of Kuantan, Pahang, Peninsular Malaysia. Geological Society of Malaysia Bulletin 13, 79–86.
Cocks, L.R.M., Torsvik, T.H., 2007. Siberia, the wandering northern terrane, and its changing geography through the Palaeozoic. Earth-Science Reviews 82 (1), 29–74.
Cogné, J.P., Kravchinsky, V.A., Halim, N., Hankard, F., 2005. Late Jurassic-Early Cretaceous closure of the Mongol-Okhotsk Ocean demonstrated by new Mesozoic palaeomagnetic results from the Trans-Baikal area (SE Siberia). Geophysical Journal International 163 (2), 813–832.
Cunningham, D., 2013. Mountain building processes in intracontinental oblique deformation belts: lessons from the Gobi Corridor, Central Asia. Journal of Structural Geology 46, 255–282.
Dash, B., Yin, A., Jiang, N., Tseveendorj, B., Han, B., 2015. Petrology, structural setting, timing, and geochemistry of cretaceous volcanic rocks in eastern Mongolia: constraints on their tectonic origin. Gondwana Research 27 (1), 281–299.
Davidson, J., Turner, S., Plank, T., 2012. Dy/Dy*: variations arising from mantle sources and petrogenetic processes. Journal of Petrology 54 (3), 525–537.
Davis, F.A., Humayun, M., Hirschmann, M.M., Cooper, R.S., 2013. Experimentally determined mineral/melt partitioning of first-row transition elements (FRTE) during

partial melting of peridotite at 3 GPa. Geochimica et Cosmochimica Acta 104, 232–260.
DePaolo, D.J., 1981. Trace element and isotopic effects of combined wallrock assimilation and fractional crystallization. Earth and Planetary Science Letters 53 (2), 189–202.
Enkhtuvshin, H., Sawada, U., Eetaya, T., Eezumee, S., 1995. A petrological study on the late Mesozoic and Cenozoic volcanic rocks of the Mongolian Plateau. Problems of Geology and Palaeontology of Mongolia 75–77.
Fan, W.M., Guo, F., Wang, Y.J., Lin, G., 2003. Late Mesozoic calc-alkaline volcanism of post-orogenic extension in the northern Da Hinggan Mountains, northeastern China. Journal of Volcanology and Geothermal Research 121 (1), 115–135.
Fan, W.M., Guo, F., Wang, Y.J., Zhang, M., 2004. Late Mesozoic volcanism in the northern Huaiyang tectono-magmatic belt, central China: partial melts from a lithospheric mantle with subducted continental crust relicts beneath the Dabie orogen? Chemical Geology 209 (1), 27–48.
Fitton, J.G., James, D., Leeman, W.P., 1991. Basic magmatism associated with late Cenozoic extension in the western United States: compositional variations in space and time. Journal of Geophysical Research - Solid Earth 96 (B8), 13693–13711.
Foley, S.F., Barth, M.G., Jenner, G.A., 2000. Rutile/melt partition coefficients for trace elements and an assessment of the influence of rutile on the trace element characteristics of subduction zone magmas. Geochimica et Cosmochimica Acta 64 (5), 933–938.
Fritzell, E.H., Bull, A.L., Shephard, G.E., 2016. Closure of the Mongol–Okhotsk Ocean: insights from seismic tomography and numerical modelling. Earth and Planetary Science Letters 445, 1–12.
Gale, A., Dalton, C.A., Langmuir, C.H., Su, Y., Schilling, J.G., 2013. The mean composition of ocean ridge basalts. Geochemistry, Geophysics, Geosystems 14 (3), 489–518.
Gao, S., Luo, T.C., Zhang, B.R., Zhang, H.F., Han, Y.W., Zhao, Z.D., Hu, Y.K., 1998. Chemical composition of the continental crust as revealed by studies in East China. Geochimica et Cosmochimica Acta 62 (11), 1959–1975.
Gao, S., Rudnick, R.L., Carlson, R.W., McDonough, W.F., Liu, Y.S., 2002. Re–Os evidence for replacement of ancient mantle lithosphere beneath the North China craton. Earth and Planetary Science Letters 198 (3), 307–322.
Gao, S., Rudnick, R.L., Xu, W.L., Yuan, H.L., Liu, Y.S., Walker, R.J., Puchtel, I.S., Liu, X., Huang, H., Wang, X.R., Yang, J., 2008. Recycling deep cratonic lithosphere and generation of intraplate magmatism in the North China Craton. Earth and Planetary Science Letters 270 (1), 41–53.
Graham, S.A., Hendrix, M.S., Johnson, C.L., Badamgarav, D., Badarch, G., Amory, J., Porter, M., Barsbold, R., Webb, L.E., Hacker, B.R., 2001. Sedimentary record and tectonic implications of Mesozoic rifting in southeast Mongolia. Geological Society of America Bulletin 113 (12), 1560–1579.
Graham, S.A., Cope, T., Johnson, C.L., Ritts, B., 2012. Sedimentary basins of the late Mesozoic extensional domain of China and Mongolia. Regional Geology and Tectonics: Phanerozoic Rift Systems and Sedimentary Basins. Elsevier Inc.
Halim, N., Kravchinsky, V., Gilder, S., Cogné, J.P., Alexyutin, M., Sorokin, A., Courtillot, V., Chen, Y., 1998. A palaeomagnetic study from the Mongol–Okhotsk region: rotated Early Cretaceous volcanics and remagnetized Mesozoic sediments. Earth and Planetary Science Letters 159 (3), 133–145.
He, L., 2014. Numerical modeling of convective erosion and peridotite-melt interaction in big mantle wedge: implications for the destruction of the North China Craton. Journal of Geophysical Research - Solid Earth 119 (4), 3662–3677.
He, L., 2015. Thermal regime of the North China Craton: implications for craton destruction. Earth-Science Reviews 140, 14–26.
Hendrix, M.S., Graham, S.A., Amory, J.Y., Badarch, G., 1996. Noyon Uul syncline, southern Mongolia: Lower Mesozoic sedimentary record of the tectonic amalgamation of central Asia. Geological Society of America Bulletin 108 (10), 1256–1274.
Herzberg, C., 2006. Petrology and thermal structure of the Hawaiian plume from Mauna Kea volcano. Nature 444 (7119), 605.
Herzberg, C., Cabral, R.A., Jackson, M.G., Vidito, C., Day, J.M.D., Hauri, E.H., 2014. Phantom Archean crust in Mangaia hotspot lavas and the meaning of heterogeneous mantle. Earth and Planetary Science Letters 396, 97–106.
Hong-fu, Zhang, Min, S., Mei-fu, Z., Wei-ming, F., Xin-hua, Z., Ming-guo, Z., 2004. Highly heterogeneous Late Mesozoic lithospheric mantle beneath the North China Craton: evidence from Sr-Nd-Pb isotopic systematics of mafic igneous rocks. Geological Magazine 141 (1), 55–62.
Hunt, A., 2011. Deciphering the Sources of Cenozoic Intra-plate Volcanism in Central Mongolia: A Geochemical Study (Doctoral dissertation, Geology).
Hunt, A.C., Parkinson, I.J., Harris, N.B.W., Barry, T.L., Rogers, N.W., Yondon, M., 2012. Cenozoic volcanism on the Hangai Dome, Central Mongolia: geochemical evidence for changing melt sources and implications for mechanisms of melting. Journal of Petrology 53 (9), 1913–1942.
Ionov, D.A., Hofmann, A.W., Shimizu, N., 1994. Metasomatism-induced melting in mantle xenoliths from Mongolia. Journal of Petrology 35 (3), 753–785.
Irvine, T.N.J., Baragar, W.R.A.F., 1971. A guide to the chemical classification of the common volcanic rocks. Canadian Journal of Earth Sciences 8 (5), 523–548.
Irwin, W.P., 2006. Geological studies in the Klamath Mountains province, California and Oregon: A volume in honor of William P. Irwin. Geological Society of America. vol. 410.
Jahn, B.M., Litvinovsky, B.A., Zanvilevich, A.N., Reichow, M., 2009. Peralkaline granitoid magmatism in the Mongolian–Transbaikalian Belt: evolution, petrogenesis and tectonic significance. Lithos 113 (3), 521–539.
Johnson, C.L., 2015. Sedimentary basins in transition: distribution and tectonic settings of Mesozoic strata in Mongolia. Geological Society of America Special Papers 513, SPE513–17.
Johnson, C.L., Greene, T.J., Zinniker, D.A., Moldowan, J.M., Hendrix, M.S., Carroll, A.R., 2003. Geochemical characteristics and correlation of oil and nonmarine source rocks from Mongolia. AAPG Bulletin 87 (5), 817–846.
Johnson, C.L., Constenius, K.C., Graham, S.A., Mackey, G., Menotti, T., Payton, A., Tully, J., 2014. Subsurface evidence for late Mesozoic extension in western Mongolia: tectonic and petroleum systems implications. Basin Research https://doi.org/10.1111/bre.12073 (p. n/a–n/a).
Johnson, C.L., Constenius, K.C., Graham, S.A., Mackey, G., Menotti, T., Payton, A., Tully, J., 2015. Subsurface evidence for late Mesozoic extension in western Mongolia: tectonic and petroleum systems implications. Basin Research 27 (3), 272–294.
Kelemen, P.B., Hanghøj, K., Greene, A.R., 2003. One view of the geochemistry of subduction-related magmatic arcs, with an emphasis on primitive andesite and lower crust. Treatise on Geochemistry 3, 659.
Kempton, P.D., Fitton, J.G., Hawkesworth, C.J., Ormerod, D.S., 1991. Isotopic and trace element constraints on the composition and evolution of the lithosphere beneath the southwestern United States. Journal of Geophysical Research - Solid Earth 96 (B8), 13713–13735.
Klemme, S., Blundy, J.D., Wood, B.J., 2002. Experimental constraints on major and trace element partitioning during partial melting of eclogite. Geochimica et Cosmochimica Acta 66 (17), 3109–3123.
Klemme, S., Prowatke, S., Hametner, K., Günther, D., 2005. Partitioning of trace elements between rutile and silicate melts: implications for subduction zones. Geochimica et Cosmochimica Acta 69 (9), 2361–2371.
Klemme, S., Günther, D., Hametner, K., Prowatke, S., Zack, T., 2006. The partitioning of trace elements between ilmenite, ulvospinel, armalcolite and silicate melts with implications for the early differentiation of the moon. Chemical Geology 234 (3), 251–263.
Kravchinsky, V.A., Cogné, J.P., Harbert, W.P., Kuzmin, M.I., 2002. Evolution of the Mongol-Okhotsk Ocean as constrained by new palaeomagnetic data from the Mongol-Okhotsk suture zone, Siberia. Geophysical Journal International 148 (1), 34–57.
Lambart, S., Laporte, D., Schiano, P., 2013. Markers of the pyroxenite contribution in the major-element compositions of oceanic basalts: review of the experimental constraints. Lithos 160, 14–36.
LeBas, M., Maitre, R.L., Streckeisen, A., Zanettin, B., IUGS Subcommission on the Systematics of Igneous Rocks, 1986. A chemical classification of volcanic rocks based on the total alkali-silica diagram. Journal of petrology 27 (3), 745–750.
Le Roux, V., Lee, C.T., Turner, S.J., 2010. Zn/Fe systematics in mafic and ultramafic systems: implications for detecting major element heterogeneities in the Earth's mantle. Geochimica et Cosmochimica Acta 74 (9), 2779–2796.
Le Roux, V., Dasgupta, R., Lee, C.T., 2011. Mineralogical heterogeneities in the Earth's mantle: constraints from Mn, Co, Ni and Zn partitioning during partial melting. Earth and Planetary Science Letters 307 (3), 395–408.
Liu, Y., Gao, S., Kelemen, P.B., Xu, W., 2008. Recycled crust controls contrasting source compositions of Mesozoic and Cenozoic basalts in the North China Craton. Geochimica et Cosmochimica Acta 72 (9), 2349–2376.
Mallik, A., Dasgupta, R., 2012. Reaction between MORB-eclogite derived melts and fertile peridotite and generation of ocean island basalts. Earth and Planetary Science Letters 329, 97–108.
Matzen, A.K., Baker, M.B., Beckett, J.R., Stolper, E.M., 2013. The temperature and pressure dependence of nickel partitioning between olivine and silicate melt. Journal of Petrology 54 (12), 2521–2545.
McKenzie, D.A.N., O'nions, R.K., 1991. Partial melt distributions from inversion of rare earth element concentrations. Journal of Petrology 32 (5), 1021–1091.
Meng, Q.R., 2003. What drove late Mesozoic extension of the northern China–Mongolia tract? Tectonophysics 369 (3), 155–174.
Menzies, M.A., Fan, W., Zhang, M., 1993. Palaeozoic and Cenozoic lithoprobes and the loss of> 120 km of Archaean lithosphere, Sino-Korean craton, China. Geological Society, London, Special Publications 76 (1), 71–81.
Menzies, M., Xu, Y., Zhang, H., Fan, W., 2007. Integration of geology, geophysics and geochemistry: a key to understanding the North China Craton. Lithos 96 (1), 1–21 (s).
Niu, Y., O'Hara, M.J., 2007. Global correlations of ocean ridge basalt chemistry with axial depth: a new perspective. Journal of Petrology 49 (4), 633–664.
Niu, Y., Collerson, K.D., Batiza, R., Wendt, J.I., Regelous, M., 1999. Origin of enriched-type mid-ocean ridge basalt at ridges far from mantle plumes: the East Pacific rise at 11 20′ N. Journal of Geophysical Research - Solid Earth 104 (B4), 7067–7087.
Pearce, J.A., 1983. Role of the Sub-continental Lithosphere in Magma Genesis at Active Continental Margins.
Rudnick, R.L., Fountain, D.M., 1995. Nature and composition of the continental crust: a lower crustal perspective. Reviews of Geophysics 33 (3), 267–309.
Samoylov, V.S., Arkelyants, M.M., 1989. The late Mesozoic magmatism of the Gobi Altai region and its structural position. Geotectonics 23, 268–275.
Şengör, A.M.C., Natal'In, B.A., Burtman, V.S., 1993. Evolution of the Altaid tectonic collage and Palaeozoic crustal growth in Eurasia. Nature 364 (6435), 299–307.
Sun, S.S., McDonough, W.S., 1989. Chemical and isotopic systematics of oceanic basalts: implications for mantle composition and processes. Geological Society, London, Special Publications 42 (1), 313–345.
Taira, A., 2001. Tectonic evolution of the Japanese island arc system. Annual Review of Earth and Planetary Sciences 29 (1), 109–134.
Thompson, R.N., Gibson, S.A., Dickin, A.P., Smith, P.M., 2001. Early cretaceous basalt and picrite dykes of the southern Etendeka region, NW Namibia: windows into the role of the Tristan mantle plume in Paraná–Etendeka magmatism. Journal of Petrology 42 (11), 2049–2081.
Tomurtogoo, O., Windley, B.F., Kröner, A., Badarch, G., Liu, D.Y., 2005. Zircon age and occurrence of the Adaatsag ophiolite and Muron shear zone, central Mongolia: constraints on the evolution of the Mongol–Okhotsk ocean, suture and orogen. Journal of the Geological Society 162 (1), 125–134.
Torsvik, T.H., Cocks, L.R.M., 2017. Earth History and Palaeogeography. Cambridge University Press, Cambridge.

Van der Voo, R., van Hinsbergen, D.J., Domeier, M., Spakman, W., Torsvik, T.H., 2015. Latest Jurassic–earliest Cretaceous closure of the Mongol-Okhotsk Ocean: a paleomagnetic and seismological-tomographic analysis. Geological Society of America Special Papers 513, 589–606.

Van Hinsbergen, D.J., Straathof, G.B., Kuiper, K.F., Cunningham, W.D., Wijbrans, J., 2008. No vertical axis rotations during Neogene transpressional orogeny in the NE Gobi Altai: coinciding Mongolian and Eurasian early Cretaceous apparent polar wander paths. Geophysical Journal International 173 (1), 105–126.

Van Hinsbergen, D.J., Cunningham, D., Straathof, G.B., Ganerød, M., Hendriks, B.W., Dijkstra, A.H., 2015. Triassic to Cenozoic multi-stage intra-plate deformation focused near the Bogd Fault system, Gobi Altai, Mongolia. Geoscience Frontiers 6 (5), 723–740.

Wang, F., Zhou, X.H., Zhang, L.C., Ying, J.F., Zhang, Y.T., Wu, F.Y., Zhu, R.X., 2006. Late Mesozoic volcanism in the Great Xing'an Range (NE China): timing and implications for the dynamic setting of NE Asia. Earth and Planetary Science Letters 251 (1), 179–198.

Windley, B.F., Alexeiev, D., Xiao, W., Kröner, A., Badarch, G., 2007. Tectonic models for accretion of the Central Asian Orogenic Belt. Journal of the Geological Society 164 (1), 31–47.

Windley, B.F., Maruyama, S., Xiao, W.J., 2010. Delamination/thinning of sub-continental lithospheric mantle under Eastern China: the role of water and multiple subduction. American Journal of Science 310 (10), 1250–1293.

Xiao, W., Windley, B.F., Sun, S., Li, J., Huang, B., Han, C., Yuan, C., Sun, M., Chen, H., 2015. A tale of amalgamation of three Permo-Triassic collage systems in Central Asia: Oroclines, sutures, and terminal accretion. Annual Review of Earth and Planetary Sciences 43, 477–507.

Xiong, X.L., Adam, J., Green, T.H., 2005. Rutile stability and rutile/melt HFSE partitioning during partial melting of hydrous basalt: implications for TTG genesis. Chemical Geology 218 (3), 339–359.

Yang, Z.F., Zhou, J.H., 2013. Can we identify source lithology of basalt? Scientific Reports 3.

Yang, Z.F., Li, J., Liang, W.F., Luo, Z.H., 2016. On the chemical markers of pyroxenite contributions in continental basalts in eastern China: implications for source lithology and the origin of basalts. Earth-Science Reviews 157, 18–31.

Yarmolyuk, V.V., Kovalenko, V.I., 2001. The Mesozoic-Cainozoic of Mongolia. In: Dergunov, A.B. (Ed.), Tectonics, Magmatism and Metallogeny of Mongolia. Taylor and Francis Group, London, pp. 203–244.

Yin, A., Nie, S.Y., 1996. 20 A Phanerozoic Palinspastic Reconstruction of China and its Neighboring Regions.

Zhang, H., Zheng, J., 2003. Geochemical characteristics and petrogenesis of Mesozoic basalts from the North China Craton: a case study in Fuxin, Liaoning Province. Chinese Science Bulletin 48 (9), 924–930.

Zhang, H.F., Sun, M., Zhou, X.H., Fan, W.M., Zhai, M.G., Yin, J.F., 2002. Mesozoic lithosphere destruction beneath the North China Craton: evidence from major-, trace-element and Sr-Nd-Pb isotope studies of Fangcheng basalts. Contributions to Mineralogy and Petrology 144 (2), 241–254.

Zhang, H.F., Sun, M., Fan, W.M., Zhou, X.H., Zhai, M.G., 2004. Highly heterogeneous Late Mesozoic lithospheric mantle beneath the North China Craton: evidence from Sr–Nd–Pb isotopic systematics of mafic igneous rocks. Geological Magazine 141 (1), 55–62.

Zorin, Y.A., 1999. Geodynamics of the western part of the Mongolia–Okhotsk collisional belt, Trans-Baikal region (Russia) and Mongolia. Tectonophysics 306 (1), 33–56.